

Dilepton and Four-Lepton Signals at the LHC in the Littlest Higgs Model with T-parity Violation

Satyanarayan Mukhopadhyay*, Biswarup Mukhopadhyaya†, Andreas Nyffeler‡

*Regional Centre for Accelerator-based Particle Physics
Harish-Chandra Research Institute
Chhatnag Road, Jhusi
Allahabad - 211 019, India*

Abstract

In the presence of the T-parity violating Wess-Zumino-Witten (WZW) anomaly term, the otherwise stable heavy photon A_H in the Littlest Higgs model with T-parity (LHT) decays to either Standard Model (SM) gauge boson pairs, or to SM fermions via loop diagrams. We make a detailed study of the collider signatures where the A_H can be reconstructed from invariant mass peaks in the opposite sign same flavor dilepton or the four-lepton channel. This enables us to obtain information about the fundamental symmetry breaking scale f in the LHT and thereby the low-lying mass spectrum of the theory. In addition, indication of the presence of the WZW term gives us hints of the possible UV completion of the LHT via strong dynamics. The crucial observation is that the sum of all production processes of heavy T-odd quark pairs has a sizeable cross-section at the LHC and these T-odd particles eventually all cascade decay down to the heavy photon A_H . We show that for certain regions of the parameter space with either a small f of around 500 GeV or relatively light T-odd quarks with a mass of around 400 GeV, one can reconstruct the A_H even at the early LHC run with $\sqrt{s} = 10$ TeV and a modest integrated luminosity of 200 pb^{-1} . At $\sqrt{s} = 14$ TeV and with an integrated luminosity of 30 fb^{-1} , it is possible to cover a large part of the typical parameter space of the LHT, with the scale f up to 1.5 TeV and with T-odd quark masses almost up to 1 TeV. In this region of the parameter space, the mass of the reconstructed A_H ranges from 66 GeV to 230 GeV.

*satya@hri.res.in

†biswarup@hri.res.in

‡nyffeler@hri.res.in

1 Introduction

Little Higgs models [1, 2] have been proposed a few years ago to explain electroweak symmetry breaking and, in particular, to solve the so-called little hierarchy problem [3]. We can view the Standard Model (SM) as an effective field theory (EFT) with a cutoff Λ and parametrize new physics in terms of higher-dimensional operators which are suppressed by inverse powers of Λ . Precision tests of the SM have not shown any significant deviations, which in turn translates into a cutoff of about $\Lambda \sim 5 - 10$ TeV which is more than an order of magnitude above the electroweak scale. Since radiative corrections to the Higgs mass are quadratically sensitive to the cutoff Λ , some amount of fine-tuning is needed to get a Higgs which is lighter than about 200 GeV as indicated by electroweak precision data.

Little Higgs models suggest a way of stabilizing the mass of the Higgs in the presence of a cut-off Λ of the above kind of magnitude. Here the Higgs particle is a pseudo-Goldstone boson of a global symmetry G which is spontaneously broken at a scale f to a subgroup H . This symmetry protects the Higgs mass from getting quadratic divergences at one loop. The electroweak symmetry is broken via the Coleman-Weinberg mechanism [4] and the Higgs mass is generated radiatively, which leads naturally to a light Higgs boson $m_H \sim (g^2/4\pi)f \approx 100$ GeV, if the scale $f \sim 1$ TeV. The little Higgs model can then be interpreted as an EFT up to a new cutoff scale of $\Lambda \sim 4\pi f \sim 10$ TeV.

Among the different versions of this approach, the littlest Higgs model [5] achieves the cancellation of quadratic divergences with a minimal number of new degrees of freedom. However, precision electroweak constraints imply that the mass scale of the new particles in such theories has to be of the order of $f \gtrsim 5$ TeV in most of the natural parameter space [6], thus necessitating fine-tuning once more. The problem is circumvented through the introduction of an additional discrete symmetry, the so-called T-parity [7, 8], whereby all particles in the spectrum are classified as T-even or T-odd. This allows one to have the Higgs mass protected from quadratic divergences, and at the same time see a spectrum of additional gauge bosons, scalars and fermions, in the mass range of a few hundred GeV, with the lightest T-odd particle (LTP), typically the heavy neutral partner of the photon, A_H , being stable. In particular, for the Littlest Higgs model with T-parity (LHT) [8, 9, 10, 11] it was shown in Refs. [10, 12, 13], that a scale f as low as 500 GeV is compatible with electroweak precision data. Furthermore, if T-parity is exact, the LTP can also be a potential dark matter (DM) candidate [9, 12, 14].

The experimental signals at colliders of a scenario with exact T-parity have close resemblance with those of supersymmetry (SUSY) with conserved R-parity or universal extra dimensions (UED) with KK-parity. First of all, T-odd particles can only be produced in pairs. Furthermore, all T-odd particles cascade decay down to the LTP which then carries away substantial missing transverse momentum, accompanied by jets and / or leptons rendered hard through the release of energy in the decay of the heavy new particles.

It was later pointed out in Ref. [15] that T-parity can be violated in the EFT by topological effects related to anomalies in the underlying theory (UV completion of the LHT). This induces a Wess-Zumino-Witten (WZW) term [16] in the low-energy effective Lagrangian, similarly to the WZW term of odd intrinsic parity in the usual chiral Lagrangian for QCD. This term encodes the Adler-Bell-Jackiw chiral anomaly [17] within the EFT framework and describes, for instance, the decay $\pi^0 \rightarrow \gamma\gamma$. The structure of the WZW term is thereby

uniquely determined by the symmetry breaking pattern $G \rightarrow H$ and the gauged subgroups, up to a multiplicative quantized constant. This constant is related to the representation of new fermions in the underlying theory, if we assume that it is strongly interacting and a fermion condensate forms which signals spontaneous symmetry breaking. Essentially, as in QCD, the prefactor of the WZW term is a function of the number of ‘colors’ in the underlying theory.

Of course, there is no such WZW term, if there are no chiral anomalies in the underlying theory, for instance, if the low-energy non-linear sigma model Lagrangian of the LHT derives from a linear sigma model with new heavy fundamental scalar fields which break the symmetry, see Ref. [18] for an explicit construction of such an UV completion with unbroken T-parity.

The phenomenology at colliders of the LHT with T-parity violation changes completely [15, 19, 21, 20]. Assuming that A_H is the LTP, the T-violating terms will lead to its decay into SM particles either directly into two electroweak gauge bosons or via one-loop graphs into SM fermion pairs. The decay width will be very small, of the order of eV. This is due to the small prefactor in front of the WZW term which counts as order p^4 in the chiral expansion, i.e. it is of the same size as one-loop effects in the EFT. Nevertheless, A_H will promptly decay inside the detector and one does therefore not expect events with large missing transverse energy. As we will see, this allows one to reconstruct the masses of the new particles, in particular of A_H itself. On the other hand, since the T-violating couplings are very small, the production mechanism of T-odd particles is essentially unchanged from the case with exact T-parity and the T-odd particles will again cascade decay down to A_H . Of course, with T-parity violation, the unstable LTP will now no longer be a suitable DM candidate.

The phenomenology of the LHT with exact T-parity at the Large Hadron Collider (LHC) has been studied quite extensively [22, 23, 24, 25]. Efforts are also on to discriminate the LHT signals from those of other scenarios where large missing E_T is predicted [26]. However, relatively few studies have taken place on the collider signals of the scenario with T-parity violation [19, 21, 20]. Although Ref. [20] gives a very comprehensive list of signals for several regions in the parameter space, definitely more detailed studies of this interesting possibility of New Physics are required, in particular, since the WZW term is a direct window into the UV completion of the LHT.

In this paper we study the decay of A_H into a pair of light leptons (electrons, muons) or, via its decay into a pair of Z -bosons, eventually into four leptons. With appropriate cuts, in particular demanding a large effective mass $M_{eff} > 1$ TeV, to reduce the SM background from $t\bar{t}$ for dileptons and ZZ for four leptons, a clear peak in the dilepton or four-lepton invariant mass distribution emerges at M_{A_H} . Since $M_{A_H} \sim f$, this will therefore allow one to directly determine the symmetry breaking scale f of the LHT with good precision. The crucial point of our analysis is the observation that since pairs of T-odd heavy quarks can be produced in strong interaction processes and since all of them eventually decay into a pair of A_H bosons and various SM particles, we get a sizeable signal at the LHC running at 10 TeV or 14 TeV, if we add all production processes of heavy T-odd quark pairs and look at the inclusive signal of $2l + X$ or $4l + X$. For the decay chain $A_H \rightarrow ZZ \rightarrow 4l$, the idea to look at the sum of all processes of T-odd heavy quark production was already proposed in Ref. [21]. Based on some rough event and detector simulations it was argued there that

a signal can be seen at the LHC, in particular, if a tight cut is applied that the four-lepton invariant mass should lie in the narrow window $M_{A_H} \pm 6$ GeV in order to reduce the SM background from ZZ . Our study will be much more detailed and we will also include the dilepton signal which will be important for A_H masses below about 120 GeV. In this respect our analysis also differs from Ref. [20] which looked into specific final states with multiple leptons and jets coming from various decay chains, but not at the total of all production processes leading to A_H .

The important points that are emphasized in this work, and where we have gone beyond the earlier studies, are as follows:

- We have performed a detailed study of two- and four-lepton signals for the situation where the LTP (the heavy photon A_H) is liable to decay. The relevant backgrounds and ways of reducing them have also been investigated.
- Our simulation shows how the mass of the A_H can be reconstructed from peaks in the dilepton and four-lepton spectra in different regions of the parameter space. This allows us to determine the fundamental parameter f in the LHT and thus gain deeper insight into the model from its low-lying particle spectrum.
- The clear identification of a decaying A_H suggests the breaking of T-parity via the WZW terms, and thus a possible UV completion of the theory in the form of a strong dynamics at a higher scale.
- The confirmation of a decaying LTP sets the scenario clearly apart from R-parity conserving SUSY or UED with conserved KK-parity. Moreover, the observation of invariant mass peaks in dilepton and four-lepton channels is not expected in R-parity violating SUSY either.

This paper is organized as follows. In Sec. 2 we briefly review some basics about the Littlest Higgs model with exact T-parity and then sketch how T-parity is violated by the WZW anomaly term, leading to an unstable A_H . Section 3 discusses the dilepton and four-lepton signal processes, starting with the parton-level production of heavy T-odd quark pairs and the decay modes and branching ratios of A_H . We also argue why the A_H is different from the often considered Z' gauge boson or the first Kaluza-Klein excitation of the graviton and thus could have escaped detection, even with a low mass of the order of 100 GeV. Finally, we present our choice of benchmark points for several values for the heavy quark masses m_{q_H} and for several values for the mass of the heavy photon M_{A_H} . Section 4 gives details on our event generation for the signal and the background. We describe the main sources of backgrounds from the SM and from within the LHT. We then go on to present our event selection criteria for the dilepton and the four-lepton signal and the various cuts to reduce the backgrounds. In Sec. 5 we present our results, first for the dilepton signal and then for the four-lepton signature. In both cases, we give numbers for the expected signal and background cross-sections after the cuts for the LHC running at a center of mass energy of 10 TeV (14 TeV) and the number of signal and background events for an integrated luminosity of 200 pb^{-1} (30 fb^{-1}). In particular, we will show that in the case where the heavy T-odd quarks are not much above the bound of approximately $m_{q_H} > 350$ GeV from Tevatron, as estimated

in Ref. [20], even with a rather modest luminosity of 200 pb^{-1} , one will get a signal in the early run of the LHC at 10 TeV. On the other hand, for T-odd quarks with masses around 1000 GeV, a clear signal will be visible with 30 fb^{-1} of integrated luminosity for the LHC running at 14 TeV. We summarize and conclude in Section 6.

2 The Littlest Higgs model with T-parity and T-parity violation

2.1 The Littlest Higgs model with T-parity

In the LHT a global symmetry $SU(5)$ is spontaneously broken down to $SO(5)$ at a scale $f \sim 1 \text{ TeV}$. An $[SU(2) \times U(1)]^2$ gauge symmetry is imposed, which is simultaneously broken to the diagonal subgroup $SU(2)_L \times U(1)_Y$, the latter being identified with the SM gauge group. This leads to four heavy gauge bosons W_H^\pm, Z_H and A_H with masses $\sim f$ in addition to the SM gauge fields. The SM Higgs doublet is part of an assortment of pseudo-Goldstone bosons which result from the spontaneous breaking of the global symmetry. This symmetry protects the Higgs mass from getting quadratic divergences at one loop, even in the presence of gauge and Yukawa interactions. The multiplet of Goldstone bosons contains a heavy $SU(2)$ triplet scalar Φ as well. In contrast to SUSY, the new states which cancel the quadratically divergent contributions to the Higgs mass due to the top quark, gauge boson and Higgs boson loops, respectively, are heavy fermions, additional gauge bosons and triplet Higgs states.

In order to comply with strong constraints from electroweak precision data on the Littlest Higgs model [6], one imposes T-parity [7] which maps the two pairs of gauge groups $SU(2)_i \times U(1)_i, i = 1, 2$ into each other, forcing the corresponding gauge couplings to be equal, with $g_1 = g_2$ and $g'_1 = g'_2$. All SM particles, including the Higgs doublet, are even under T-parity, whereas the four additional heavy gauge bosons and the Higgs triplet are T-odd. The top quark has two heavy fermionic partners, T_+ (T-even) and T_- (T-odd). For consistency of the model, one has to introduce the additional heavy, T-odd vector-like fermions u_H^i, d_H^i, e_H^i and ν_H^i ($i = 1, 2, 3$) for each SM quark and lepton field. For further details on the LHT, we refer the reader to Refs. [8, 9, 10, 11].

The masses of the heavy gauge bosons in the LHT are given by

$$M_{W_H} = M_{Z_H} = gf \left(1 - \frac{v^2}{8f^2} \right) \approx 0.65f, \quad M_{A_H} = \frac{fg'}{\sqrt{5}} \left(1 - \frac{5v^2}{8f^2} \right) \approx 0.16f, \quad (1)$$

where corrections of $\mathcal{O}(v^2/f^2)$ are neglected in the approximate numerical values. Thus these particles have masses of several hundreds of GeV for $f \sim 1 \text{ TeV}$, although A_H , the heavy partner of the photon, can be quite light, because of the small prefactor, and is usually assumed to be the LTP. The masses of the heavy, T-odd fermions are determined by general 3×3 mass matrices in the (mirror) flavor space, $m_{q_H, l_H}^{ij} \sim \kappa_{q, l}^{ij} f$ with $i, j = 1, 2, 3$. We simplify our analysis by assuming that $\kappa_q^{ij} = \kappa_q \delta^{ij}$. The parameter $\kappa_q \sim \mathcal{O}(1)$ thus determines the masses of the heavy quarks in the following way:

$$m_{u_H} = \sqrt{2}\kappa_q f \left(1 - \frac{v^2}{8f^2} \right), \quad m_{d_H} = \sqrt{2}\kappa_q f, \quad (2)$$

thereby allowing the new heavy quarks to have masses ranging from several hundreds of GeV to a TeV, for $f \sim 1$ TeV. Similarly, the masses of the heavy leptons in the spectrum are determined by a common parameter κ_l . Note that these heavy quarks and leptons cannot be decoupled from the model as there is an upper bound $\kappa \leq 4.8$ (for $f = 1$ TeV) obtained from 4-fermion operators [10]. We will come back to lower limits on the masses of the heavy quarks and therefore on κ_q in the context of the model with T-parity violation.

While they can act as a source of model background for our leptonic signals, the T-odd leptons do not otherwise play any important role in our analysis. We will therefore use $\kappa_l = 1$ throughout. In the section on background analysis, we discuss the model backgrounds in further detail. Thus f and κ_q determine the part of the LHT spectrum relevant for our study. The mass of the triplet scalar Φ is related to the doublet Higgs mass by $m_\Phi = \sqrt{2}m_H f/v$. We will take $m_H = 120$ GeV throughout this paper. Two more dimensionless parameters λ_1 and λ_2 appear in the top quark sector; the top mass being given by $m_t = (\lambda_1/\sqrt{1+R^2})v$, where $R = \lambda_1/\lambda_2$. The masses of the two heavy partners of the top quark, T_+ and T_- , can be expressed as $m_{T_+} = \lambda_2\sqrt{1+R^2}f$ and $m_{T_-} = \lambda_2 f$. We use $m_t = 175$ GeV in our analysis and set $R = 1$.

2.2 T-parity violation

T-parity violation in the LHT and thus the decay of the heavy photon A_H arises via the so-called Wess-Zumino-Witten term [16], which, according to Ref. [15], can be written as follows:

$$\Gamma_{\text{WZW}} = \frac{N}{48\pi^2} (\Gamma_0[\Sigma] + \Gamma[\Sigma, A_l, A_r]). \quad (3)$$

The functional $\Gamma_0[\Sigma]$ is the ungauged WZW term which depends only on the non-linear sigma model field Σ . It cannot be expressed as a four-dimensional integral over a local Lagrangian. Instead, a closed form can be written as an integral over a five-dimensional manifold with ordinary spacetime as its boundary [16]. The term $\Gamma[\Sigma, A_l, A_r]$ is the gauged part of the WZW term. This part can be written as an ordinary four-dimensional integral over a local Lagrangian. The explicit expressions for the functionals and the relation of the fields $A_{l,r}$ to the gauge fields in the LHT can be found in Ref. [15]. While these functionals are uniquely given by the symmetry breaking pattern $SU(5) \rightarrow SO(5)$ and the gauged subgroups in the LHT, the integer N in Eq. (3) depends on the UV completion of the LHT. In strongly coupled underlying theories it will be related to the representation of the fermions whose condensate acts as order parameter of the spontaneous symmetry breaking. In the simplest case, N will simply be the number of ‘colors’ in that UV completion, as is the case for the WZW term in ordinary QCD. The overall coefficient $N/48\pi^2$ encapsulates the effect of the chiral anomaly, which is a one-loop effect in the corresponding high-scale theory.

As noted in Ref. [15], the WZW term in Eq. (3) is not manifestly gauge invariant. Gauge invariance is violated by terms with three or four gauge bosons with an odd number of T-odd gauge bosons, e.g. by a term like $\epsilon_{\mu\nu\rho\sigma} V_H^\mu V^\nu \partial^\rho V^\sigma$, where V_H is a T-odd gauge boson and V denotes a SM gauge boson. Such anomalous terms need to be cancelled to have a consistent theory and some mechanisms to achieve this are discussed in Ref. [15]. After this cancellation, the leading T-odd interactions appear only at order $1/f^2$. For instance, we get a vertex with

one T-odd gauge boson and two SM gauge bosons from $\epsilon_{\mu\nu\rho\sigma}(H^\dagger H/f^2)V_H^\mu V^\nu \partial^\rho V^\sigma$, after the Higgs doublet H gets a vacuum expectation value v .

To leading order in $1/f$, the part of the WZW term containing one neutral T-odd gauge boson is given, in unitary gauge, by

$$\Gamma_n = \frac{Ng^2g'}{48\pi^2f^2} \int d^4x (v+h)^2 \epsilon_{\mu\nu\rho\sigma} \times$$

$$\left[-(6/5)A_H^\mu (c_w^{-2}Z^\nu \partial^\rho Z^\sigma + W^{+\nu}D_A^\rho W^{-\sigma} + W^{-\nu}D_A^\rho W^{+\sigma} + i(3gx_w + g's_w)W^{+\nu}W^{-\rho}Z^\sigma) \right.$$

$$\left. + t_w^{-1}Z_H^\mu (2c_w^{-2}Z^\nu \partial^\rho Z^\sigma + W^{+\nu}D_A^\rho W^{-\sigma} + W^{-\nu}D_A^\rho W^{+\sigma} - 2i(2gc_w + g's_w)W^{+\nu}W^{-\rho}Z^\sigma) \right]. \quad (4)$$

Here h is the physical Higgs boson, $D_A^\mu W^{\pm\nu} = (\partial^\mu \mp ieA^\mu)W^{\pm\nu}$ and s_w, c_w and t_w denote the sine, cosine and tangent of the weak mixing angle, respectively. All T-violating vertices with up to four legs have been tabulated in Ref. [20] and implemented into a model file for CalcHEP 2.5 [27, 28].

If A_H is heavy, the vertices in Eq. (4) lead to its decay into a pair of Z -bosons or into W^+W^- with a decay width of the order of eV [19]. On the other hand, if $M_{A_H} < 2M_W$, the heavy photon cannot decay into on-shell SM gauge bosons. It could still decay into (one or two) off-shell SM gauge bosons, but for low masses loop induced decays into SM fermions will dominate. In fact, as discussed in Ref. [20], the T-violating vertices can couple the A_H to two SM fermions via a triangle loop. But since the corresponding one-loop diagrams are logarithmically divergent, one needs to add counterterms to the effective Lagrangian of the form

$$\mathcal{L}_{\text{ct}} = \bar{f}\gamma_\mu \left(c_L^f P_L + c_R^f P_R \right) f A_H^\mu, \quad (5)$$

$$c_i^f = c_{i,\epsilon}^f \left(\frac{1}{\epsilon} + \log(\mu^2) + \mathcal{O}(1) \right), \quad (6)$$

where $P_{L,R} = (\mathbf{1} \mp \gamma_5)/2$. As shown in Ref. [20] the counterterms can also be written in a manifestly gauge invariant way. These counterterms are only some of the infinitely many terms which have to be included anyway at higher orders in the momentum and loop expansion in the EFT. This procedure to renormalize the EFT order by order is well known from chiral perturbation theory [29] and, as usually done there, dimensional regularization was used in Ref. [20] which preserves chiral and gauge invariance.¹

The coefficients $c_i^f(\mu)$ of the counterterms can be estimated by naive dimensional analysis [31] or naturalness arguments. Since the scale dependence of the loop diagrams is cancelled by the scale dependence of the counterterms $c_i^f(\mu)$, any change of order one in the renormalization scale should be compensated by a change of order one in $c_i^f(\mu)$. Therefore these coefficients are given, up to $\mathcal{O}(1)$ factors, by the coefficients of the leading $1/\epsilon$ divergence in dimensional regularization of the loop integrals. The coefficients $c_{i,\epsilon}^f$ are explicitly listed in Ref. [20] and we have included the vertices from Eq. (5) in the CalcHEP model file.

¹Of course, in view of the notorious problems with dimensional regularization in chiral gauge theories and the appearance of γ_5 and the Levi-Civita tensor $\epsilon_{\mu\nu\rho\sigma}$, for a consistent treatment of divergent loop integrals a more appropriate regularization scheme should be chosen like the proper-time method or zeta-function regularization, see Ref. [30].

The finite parts of the counterterms are determined by the underlying theory. For a given UV completion of the LHT, they can be obtained, in principle, by integrating out the new ‘resonances’ which lie above the cutoff Λ of the LHT. Since the branching ratios (BR’s) into the different SM fermions depend on these coefficients, at least in principle, we could get information on the UV completion of the LHT by precisely measuring the BR’s of A_H . We will discuss below, how $\mathcal{O}(1)$ changes (different for quarks and leptons) in the coefficients $c_{i,\epsilon}^f$ could affect these BR’s and thus our analysis. Note that the unknown constant N from Eq. (4) cancels in the branching ratios. Actually, if we could measure the total decay width of A_H , we could even get information on N itself, in the same way as the decay $\pi^0 \rightarrow \gamma\gamma$ yields information about the number of colors in ordinary QCD, however, the width of $\mathcal{O}(\text{eV})$ for A_H is too small to be measurable.

The prefactor of the WZW term, $N/48\pi^2$, is of the size of a one-loop effect, thus the coupling of A_H and other T-odd gauge bosons to SM fermions via a triangle-loop is effectively 2-loop suppressed. Therefore these T-violating couplings will not affect the production mechanism of T-odd particles and their cascade decays at colliders, or EW precision observables [20]. In particular, T-parity violation should still satisfy the EW data with a rather small scale f . It is only in decays of the A_H that the anomaly term acquires phenomenological importance. As we demonstrate in what follows, reconstruction of the A_H mass becomes possible through such decays, thus confirming the bosonic nature of the LTP.

Since there is no stable LTP now, the collider signals in the LHT with T-parity violation are completely different from the LHT with exact T-parity. The LEP bounds of order 100 GeV still apply to all T-odd particles except for the A_H . In addition, based on an analysis of recent Tevatron data from CDF Vista on multijet events [32], it has been argued in Ref. [20] that a bound of $m_{q_H} > 350$ GeV applies to the LHT with broken T-parity.

3 The dilepton and four-lepton signal processes

3.1 Parton level production of heavy T-odd quark pairs

As the cross-section for direct single or pair production of A_H is very tiny, this gauge boson can essentially only be produced via the decay of heavier T-odd particles. Hence, in principle, we should be considering the production of all such T-odd particle pairs and their subsequent decays. But owing to the substantial technical difficulties in simulating all such processes together, we restrict our attention to the production of heavy T-odd quarks in the initial parton level hard scattering. Needless to say, our cross-sections for the specific final states that we consider are then rather underestimated, and can be taken as lower bounds.

We consider the following processes for the production of T-odd quark pairs at the LHC:

$$pp \rightarrow q_H \bar{q}_H + X, \quad \text{where } q_H = u_H, d_H, c_H, s_H, b_H, t_H, \quad (7)$$

$$pp \rightarrow u_H u_H + X, \quad \bar{u}_H \bar{u}_H + X, \quad d_H d_H + X, \quad \bar{d}_H \bar{d}_H + X, \\ u_H d_H + X, \quad \bar{u}_H \bar{d}_H + X, \quad u_H \bar{d}_H + X, \quad (8)$$

where t_H denotes the lighter T-odd partner of the top quark. Since, T_- , the heavier T-odd partner of the top quark has a mass of 1013 GeV (for $f = 1$ TeV) and is thus heavier than t_H (for most of our choices for κ_q below), its cross-section is much smaller and we have

neglected its pair production. Of course, for lower values of f , both $T_-\bar{T}_-$ and heavy T-odd gauge boson productions can have appreciable cross-section at the LHC.

In general, we expect the processes in Eq. (7) to be dominant because of the strong interaction production channels through gluon-gluon fusion and $q\bar{q}$ -annihilation. But the electroweak processes from Eq. (8) also contribute significantly to the cross-section via t -channel T-odd gauge boson exchange, especially when the T-odd gauge bosons become relatively light, i.e. for low values of f . For instance, for $f = 1$ TeV and $\kappa_q = 0.5$, we find $m_{q_H} \sim 700$ GeV and the total production cross-section for a pair of heavy T-odd quarks is about 2.1 (0.7) pb for the LHC running at 14 (10) TeV. On the other hand, we can also obtain $m_{q_H} \sim 700$ GeV by choosing $f = 500$ GeV and $\kappa_q = 1$. In this later case the cross-section goes up to 5.8 (2.3) pb, where actually the electroweak processes from Eq. (8) are found to dominate. This fact has also been observed recently in Ref. [25]. We will come back to this point below. If the heavy T-odd quarks do not lie much above the lower bound of $m_{q_H} > 350$ GeV, we get a cross-section of 36 (13) pb for $m_{q_H} \sim 400$ GeV with $f = 1$ TeV. For details on the production of the heavy quarks and the relevant plots for the variation of these cross-sections with f or m_{q_H} , we refer the reader to the Refs. [22, 23]. We have checked that for individual processes, our results agree with them. Note, however, as f determines the mass of A_H , and in turn its decay modes, in order to study the effect of variation of quark masses with M_{A_H} fixed, in some cases we vary κ_q to adjust the masses of the heavy T-odd quarks.

The important fact is that the sum of the cross-sections of all T-odd quark pair production processes can be sizeable, in particular for not too large m_{q_H} . This will allow us to extract a clear signal after cuts are applied. Furthermore, since additional electroweak processes which can, for instance, produce pairs of T-odd gauge bosons $V_H V_H$, finally also lead to two A_H 's, the given cross-sections, as mentioned before, are actually rather lower bounds.

The initially produced T-odd heavy quarks subsequently decay as $q_H \rightarrow W_H q'$, $Z_H q$, $A_H q$ and then $W_H \rightarrow A_H W$, $\bar{q} q'_H$ and $Z_H \rightarrow A_H h$, $q \bar{q}_H$. At one point in such decay chains of a pair of q_H 's, we are left with two A_H bosons, which will further decay as discussed in the next subsection. There will also be several hard jets and leptons and some amount of missing E_T , if there are decays of W^\pm and Z into neutrinos.

The initial parton level hard-scattering matrix elements and the relevant decay branching ratios for the signal in the LHT with T-parity violation are calculated with the help of CalcHEP (Version 2.5.1) [27]. We have used the CalcHEP model files for the LHT (with exact T-parity) from Ref. [23]² and the one from Refs. [20, 28] for the T-violating terms. We have used the leading order CTEQ6L [34] parton distribution functions with NLO running of α_s with $\alpha_s(M_Z) = 0.118$. The QCD factorization and renormalization scales were set equal to the sum of the masses of the particles which are produced in the initial parton level scattering process.

²A new CalcHEP model file has been written by the authors of Ref. [25] which includes some missing factors of order v^2/f^2 in the couplings of T-odd fermions to the Z - and W -bosons, which were found in Ref. [33]. These changes in the Feynman rules will, however, not significantly affect our analysis, which focuses on the decays of the A_H boson.

3.2 Decay modes of A_H

A comprehensive list of possible final states in the LHT with T-parity violation after the decay of the A_H 's is given in Ref. [20]. Here we are interested in either dilepton or four-lepton signals from the decay of the two A_H 's. The advantage of these leptonic decay channels of A_H is very apparent. As we will see, one can obtain clean signatures over the backgrounds with a minimal number of selection cuts and with luminosity building up, clear peaks in the invariant-mass distributions of dileptons or four leptons give us information about the A_H mass and thus on the symmetry breaking scale f . The decay branching fractions of A_H to either leptons (electron, muon) or to a pair of Z bosons (one of which might be off-shell) are given in Table 1. Note that the BR for the further decay $ZZ \rightarrow l^+l^-l'^+l'^-$, where $l, l' = \{e, \mu\}$, is only 4.5×10^{-3} , but the signal in this channel is very clean and the SM backgrounds, primarily from ZZ production, can be reduced efficiently as we will discuss below.

f (GeV)	M_{A_H} (GeV)	$\text{BR}(A_H \rightarrow e^+e^-) + \text{BR}(A_H \rightarrow \mu^+\mu^-)$ (%)	$\text{BR}(A_H \rightarrow ZZ^{(*)})$ (%)
500	66	7.59	~ 0
750	109	7.40	0.18
1000	150	3.42	11.03
1100	166	0.99	8.67
1500	230	0.02	22.45

Table 1: Decay branching fractions of A_H to leptons ($l = e, \mu$) or $ZZ^{(*)}$ as a function of the scale f , i.e. the mass M_{A_H} .

As already observed in Ref. [20], for lower masses ($M_{A_H} \lesssim 120$ GeV, $f \lesssim 800$ GeV) the decay of A_H is dominated by the loop-induced two-body modes into fermions, whereas for higher masses ($M_{A_H} > 2M_W$, $f > 1070$ GeV) the two-body modes to gauge boson pairs dominate. For intermediate masses, both the two-body and three-body modes compete (in the three-body mode we have one on-shell W^\pm or Z). The decay into two off-shell Z 's for low f will have a very small branching-fraction, as the relative one-loop suppression is already compensated by the off-shellness of one vector boson.

As mentioned earlier, the decay rates of A_H into fermions (quarks, charged leptons, neutrinos) via one-loop triangle diagrams depend on the values of the finite terms in the counterterms from Eq. (5). To obtain the results given in Table 1 we followed Ref. [20] and used naive dimensional analysis to fix the $\mathcal{O}(1)$ constants from Eq. (6) to be exactly equal to one. These finite terms are determined by the UV completion of the LHT and could easily be different from one. In particular, one could imagine a situation, where the underlying theory couples differently to quarks and leptons. For instance, it could happen that all the couplings of the charged leptons could be bigger by a factor of two, which is well within the uncertainty of naive dimensional analysis. This would increase the partial decay width $\Gamma(A_H \rightarrow \text{all charged leptons})$ by a factor of four. The corresponding change of the branching ratio $\text{BR}(A_H \rightarrow e^+e^-) + \text{BR}(A_H \rightarrow \mu^+\mu^-)$, which is relevant for our study, depends on the total decay width and therefore on the mass of A_H or the scale f .

It increases by about a factor of three for $M_{A_H} = M_Z$, i.e. for $f = 650$ GeV. Such a scenario would of course require less luminosity to get a certain number of dilepton events in our analysis below. On the other hand, if the underlying theory increases the couplings of A_H to only the quarks by a factor of two compared to naive dimensional analysis, then the $\text{BR}(A_H \rightarrow e^+e^-) + \text{BR}(A_H \rightarrow \mu^+\mu^-)$ would be smaller (by a factor of about three for $M_{A_H} = M_Z$) and we would need more luminosity. While the precise numbers for these fermionic branching ratios therefore crucially depend on the unknown $\mathcal{O}(1)$ coefficients in the counterterms, the overall results of our analysis are not expected to change. In particular, the required luminosity is not expected to change by more than a factor of three, up or down.

As already noted in Ref. [20] as soon as the $WW^{(*)}$ and $ZZ^{(*)}$ decay channels for A_H open up for larger M_{A_H} or f , they quickly dominate over the fermionic modes. Therefore the overall picture and the value of f where this cross-over occurs, does not depend too sensitively on the precise values of the counterterms, as long as they vary only in a reasonably small window around the values as predicted by naive dimensional analysis.

3.3 Why is the A_H different from a usual Z' ?

Of course, the strategy to look for a resonance peak in the invariant mass distribution of dileptons is well known from the searches for a Z' gauge boson which appears in many models of New Physics, see for instance the recent reviews [35] and references therein.

Low energy weak neutral current experiments are affected by Z' exchange, which is mainly sensitive to its mass, and by $Z - Z'$ mixing. On the other hand, measurements at the Z -pole are very sensitive to $Z - Z'$ mixing, which lowers the mass of the Z relative to the SM prediction and also modifies the $Zf\bar{f}$ vertices. For e^+e^- colliders, like LEP2, a Z' much heavier than the center of mass energy would manifest itself through induced four-fermion interactions, which then interfere with virtual γ and Z contributions for leptonic and hadronic final states. The primary discovery mode at hadron colliders, like the Tevatron, is from the direct Drell-Yan production of a dilepton resonance.

The bounds on the Z' mass in a variety of popular models are usually obtained by assuming the Z' coupling to SM fermions to be of electroweak strength and family universal. Then for some models the strongest bounds come from electroweak precision tests yielding $M_{Z'} \gtrsim 1200 - 1400$ GeV at 95% confidence level. On the other hand, for a sequential Z' model, the LEP2 lower bound is even around 1800 GeV. For other models, the bounds from direct searches at the Tevatron are better than those derived from electroweak data, typically one obtains $M_{Z'} \gtrsim 800 - 1000$ GeV for these models [35].

Why does this fact not rule out a A_H with a mass around 50 – 250 GeV which we will consider below ? The crucial point is that although a light A_H decays with a large BR into a pair of SM fermions, the actual coupling of A_H to two SM fermions is very small. Essentially, the coupling is of the size of a two-loop effect as discussed above. Thus the couplings are very different from the most commonly considered Z' models with couplings of electroweak strength for which the above limits apply. Therefore the direct production cross-section of such a low-mass A_H in e^+e^- colliders like LEP2 or at the Tevatron is tiny, of the order of 10^{-6} pb [20]. Also the four-fermion operators induced by Z' at low energies have only a small coupling and will not affect low-energy weak observables. Furthermore, the coupling of A_H to WW or ZZ which is directly induced by the WZW term, see Eq. (4),

is very small and thus the production cross-section for A_H radiated off some W or Z boson is again very small. Therefore the A_H cannot be produced directly, but only via the decay of heavier T-odd particles, which themselves have not yet been observed.

As far as the decay $A_H \rightarrow ZZ$ is concerned, again the small coupling of A_H to SM fermions leads to a tiny s -channel production cross-section at LEP2 or the Tevatron. This is in contrast to the case of models with warped extra dimensions, like Randall-Sundrum (RS) [36], where the first Kaluza-Klein excitation of the graviton, G_1 , can have a sizeable coupling to SM fermions and also often decays into ZZ with a branching ratio of typically 5%. From the absence of any deviation from the SM signal in $e^+e^- \rightarrow ZZ$ at LEP2 it was concluded in Ref. [37] that $M_{G_1} > 700$ GeV. Recently, CDF [38] has searched for a new heavy particle decaying to $ZZ \rightarrow eeee$ in the mass range of 500 – 1000 GeV. In 1.1 fb^{-1} of integrated luminosity, no event was observed after all the selection cuts, with an expected background of 0.028 ± 0.014 events. Within the RS-model, this translates into $\sigma(p\bar{p} \rightarrow G_1) \times \text{BR}(G_1 \rightarrow ZZ) < 4 \text{ pb}$ at 95% C.L. for $M_{G_1} \sim 500$ GeV. Since the mass region below 400 GeV was used to control the background from hadrons faking electrons, a potential signal from a lighter resonance, like the A_H with a mass around 150 – 250 GeV, could not be observed. In any case, no signal is expected, since for a A_H of mass 230 GeV, produced in cascade decays of T-odd quarks with mass 400 GeV, $\sigma(p\bar{p} \rightarrow A_H) \times \text{BR}(A_H \rightarrow ZZ) = 0.03 \text{ pb}$. This is well below the above bound. A light A_H with a mass well below 1 TeV, giving a simultaneous signal in the dilepton and four-lepton channels (via ZZ), also sets the LHT with T-parity violation apart from R-parity violating SUSY models with an additional Z' which can decay into four leptons via a slepton/sneutrino pair, as proposed in Ref. [39].

3.4 Choice of benchmark points

As discussed above, the production cross-section of heavy T-odd quark pairs decreases with increasing mass m_{q_H} , up to the discussed enhancement of the electroweak processes from Eq. (8) for low f . We therefore will choose benchmark points (BP's) with $m_{q_H} \sim 400, 700, 1000$ GeV to see this effect. The point with the lightest mass is close to the bound $m_{q_H} > 350$ GeV found in Ref. [20] from recent Tevatron data.

The intermediate mass region $120 \text{ GeV} < m_{A_H} < 165 \text{ GeV}$ ($800 \text{ GeV} < f < 1100 \text{ GeV}$) will be the most difficult to analyze, since neither the BR of A_H into dileptons nor into four leptons (via ZZ) dominates as can be seen from Table 1. Therefore we first take a benchmark point from this region and choose $f = 1 \text{ TeV}$ which corresponds to $M_{A_H} = 150 \text{ GeV}$. Later, we will also take $f = 500 \text{ GeV}$, where the dilepton mode dominates and $f = 1500 \text{ GeV}$, where the dilepton mode is negligible and the decay into ZZ and thus into four leptons is important.

The first two BP's with $f = 1 \text{ TeV}$ are chosen in order to illustrate the effect of low and heavy quark masses both at the production level and at the level of kinematical variables. We take for the first BP-1 $m_{q_H} = 400 \text{ GeV}$ ($\kappa_q = 0.285$) and for the second BP-2 $m_{q_H} = 700 \text{ GeV}$ ($\kappa_q = 0.5$), see Table 2.

As we will see below, BP-1 with a rather low m_{q_H} leads to a clean dilepton signal over the backgrounds with rather modest luminosity. Therefore such a scenario should be testable during the early run of the LHC with 10 TeV center of mass energy, even in the difficult

intermediate mass region for M_{A_H} . We expect the analysis to be easier for either lighter M_{A_H} (lower f) or heavier M_{A_H} (higher f), where one of the dilepton or four-lepton signals will clearly dominate.

For the further BP's, we therefore restrict ourselves to the heavier quark masses $m_{q_H} \sim 700, 1000$ GeV. For $m_{q_H} \sim 700$ GeV, we show the possible reconstruction of the A_H mass in the invariant mass distributions of dileptons for a point with very low values of $f = 500$ GeV ($M_{A_H} = 66$ GeV) (BP-3) and of four leptons for a point with a higher value of $f = 1500$ GeV ($M_{A_H} = 230$ GeV) (BP-4), see Table 2. As the T-odd quarks become heavier, their production cross-section goes down. It then becomes increasingly difficult to obtain a reasonable number of signal events over the background. In such a scenario, in order to check the reach of the LHC, we choose the last two benchmark points such that $m_{q_H} \sim 1000$ GeV. For reasons discussed above, here also we consider two different values of f , $f = 1000$ GeV ($M_{A_H} = 150$ GeV) (BP-5) and $f = 1500$ GeV ($M_{A_H} = 230$ GeV) (BP-6).

Benchmark Point	m_{d_H} (GeV)	m_{u_H} (GeV)	M_{A_H} (GeV)	f (GeV)	κ_q	$\sqrt{s} = 10$ TeV $\sigma_{q_H q_H}$ (fb)	$\sqrt{s} = 14$ TeV $\sigma_{q_H q_H}$ (fb)
BP-1	403	400	150	1000	0.285	12764.6	35989.0
BP-2	707	702	150	1000	0.5	660.8	2061.0
BP-3	707	686	66	500	1.0	2298.1	5750.4
BP-4	742	740	230	1500	0.35	373.0	1283.1
BP-5	1025	1018	150	1000	0.725	119.9	421.0
BP-6	1008	1004	230	1500	0.475	66.3	261.0

Table 2: The different benchmark points (BP's) for our study. These choices are made in view of the different scenarios that can arise in terms of production cross-sections, decay branching fractions and kinematic distributions. We also present the heavy quark pair production cross-section $\sigma_{q_H q_H}$ for the sum of all parton-level processes from Eqs. (7) and (8) at the LHC with center of mass energies of 10 TeV and 14 TeV.

In Table 2 we have also listed the total production cross-section for the sum of all parton-level processes from the strong-interaction processes from Eq. (7) and the electroweak processes from Eq. (8) at the LHC with center of mass energies of 10 TeV and 14 TeV. For BP-2, the strong interaction processes dominate and yield about 1.47 pb, while the electroweak processes give only a contribution of 0.60 pb at 14 TeV, i.e. about 29%. On the other hand, for BP-3 with low $f = 500$ GeV and therefore rather light A_H, Z_H (exchanged in the t -channel), the electroweak processes contribute 3.75 pb at a center of mass energy of 14 TeV, i.e. 65% of the total, compared to 2.0 pb from strong interaction processes. The biggest individual parton-level cross-section is $\sigma(pp \rightarrow u_H d_H + X) = 2.39$ pb. This has to be compared with the QCD process $\sigma(pp \rightarrow u_H \bar{u}_H + X) = 0.44$ pb from $q\bar{q}$ -annihilation and gluon-fusion, the latter contributing about one third. The relative smallness of the QCD processes can be understood from the small value of $\alpha_s(\mu_R = 2m_{q_H} = 1.4 \text{ TeV}) = 0.084$ and the size of the various parton density functions for $\mu_F = 2m_{q_H} = 1.4 \text{ TeV}$ around $x \sim m_{q_H}/7 \text{ TeV} = 0.1$.

4 Event generation: backgrounds and signal event selection

As noted earlier, the initial parton level hard-scattering matrix elements in the LHT with T-parity violation were calculated and the events generated with the help of CalcHEP. These events, along with the relevant masses, quantum numbers and two-body and three-body decay branching fractions were passed on to PYTHIA (Version 6.421) [40] with the help of the SUSY Les Houches Accord (SLHA) (v1.13) SUSY/BSM spectrum interface [41] for their subsequent decays, showering, and hadronization. Initial and final state radiations from QED and QCD and multiple interactions were also taken into account in PYTHIA. The SM backgrounds, except for $Z^{(*)}/\gamma^*$ (Drell-Yan process), were simulated with ALPGEN [42] and then subsequently the unweighted event samples are passed onto PYTHIA for their showering and hadronization. The matching of matrix-element hard partons and shower-generated jets is performed using the MLM prescription [42]. This jet-parton matching allows us to generate inclusive samples of arbitrary jet multiplicity without any over-counting. Owing to the very large cross-section for the Drell-Yan process, it was not possible to generate statistically significant samples of events with additional hard jets using ALPGEN. Instead, the Drell-Yan background has been simulated with PYTHIA. As we will explain below, after appropriate cuts, the Drell-Yan background is reduced to a negligible level. We have again used the leading order CTEQ6L parton distribution functions (for PYTHIA we use the Les Houches Accord Parton Density Function (LHAPDF) interface [43]). The QCD factorization and renormalization scales are in general kept fixed at the sum of the masses of the particles which are produced in the initial parton level scattering process. For the production of $Z^{(*)}/\gamma^*$, we have chosen the scale to be M_Z . If we would decrease the QCD scales by a factor of two, the cross-section can increase by about 30%.

4.1 Background from SM processes and within the LHT

The main SM backgrounds for the dilepton channel come from the Drell-Yan process via $Z^{(*)}/\gamma^*$ and the abundantly produced top quark pairs, whereas for the four-lepton channel, ZZ is the dominant source of background.³ For the dilepton channel we have also considered the backgrounds coming from ZZ, ZW, WW and tW . We have included additional multiple hard jets in the simulations as follows:

- $t\bar{t} + n$ jets, $0 \leq n \leq 4$
- $ZZ + n$ jets, $0 \leq n \leq 3$
- $ZW + n$ jets, $0 \leq n \leq 3$
- $WW + n$ jets, $0 \leq n \leq 3$

³Although $t\bar{t}$ events can also give rise to four-lepton events, such backgrounds are relatively easily reduced with the requirement that among the four leptons, there are at least two opposite sign same flavor ones, whose invariant mass is around the Z boson mass, followed by the effective mass cut, as shown in our subsequent analysis.

- $tW + n$ jets, $0 \leq n \leq 1$

For the other possible dilepton and four-lepton backgrounds, we have checked that their cross-sections are small compared to the above ones, for instance, for $t\bar{t}Z$, where $Z \rightarrow l^+l^-$, the cross-section is around 40 fb at $\sqrt{s} = 14$ TeV.⁴ After putting a large effective mass cut as described below, these backgrounds are not expected to be significant. Additional leptons coming from the photons radiated by charged particles, or from the decay of pions, are generally expected to be removed by the basic isolation cuts described later.

For the strongly produced process $t\bar{t} +$ jets, which has a long tail in the effective mass distribution, we have multiplied the leading order cross-sections from ALPGEN by appropriate K-factors wherever they are available in the literature. For $t\bar{t} + 0$ jet the K-factor used is 2.2 from next-to-leading order (NLO) and next-to-leading-log resummed (NLL) corrections according to the analysis in Ref. [44]. For $t\bar{t} + 1$ jet we have used a K-factor of 1.29 according to the NLO calculation in Ref. [45], whereas for $t\bar{t} + 2$ jets we used 1.28 as inferred from the recent NLO calculation in Ref. [46].⁵

In addition, two-and four-lepton final states can occur from processes within the LHT model itself. The heavy T-odd gauge bosons, W_H and Z_H , produced in various cascades, can lead to hard isolated leptons. Leptons from b-quarks and τ 's in LHT cascades can also fake our signals *prima facie*. For small κ_l , T-odd leptons l_H will also give rise to leptons in the final state. Since we have taken $\kappa_l = 1$, the latter decay does not occur for the chosen benchmark points. On the whole, substantial as several of the aforementioned backgrounds may be, they do not in general affect the invariant mass peaks from A_H decays.

4.2 Event selection criteria

In our analysis we demand for the *dilepton signal* that we have exactly one pair of opposite sign same flavor (OSSF) leptons from the decay $A_H \rightarrow l^+l^-$, with $l = \{e, \mu\}$. For the *four-lepton signal* from the decay $A_H \rightarrow ZZ^{(*)} \rightarrow l^+l^-l'^+l'^-$, where $l, l' = \{e, \mu\}$, we demand that there should be four leptons, among which at least one OSSF lepton pair should have an invariant mass peaked around M_Z (i.e., $M_Z - 20 \text{ GeV} \leq M_{ll} \leq M_Z + 20 \text{ GeV}$). The last criterion is used because in the scenarios that we consider, at least one Z -boson is on-shell.

The following basic selection cuts (denoted by Cut-1 below) were applied for both the signal and the background [48, 49]:

Lepton selection:

- $p_T > 10$ GeV and $|\eta_\ell| < 2.5$, where p_T is the transverse momentum and η_ℓ is the pseudorapidity of the lepton (electron or muon).
- **Lepton-lepton separation:** $\Delta R_{\ell\ell} \geq 0.2$, where $\Delta R = \sqrt{(\Delta\eta)^2 + (\Delta\phi)^2}$ is the separation in the pseudorapidity–azimuthal angle plane.
- **Lepton-jet separation:** $\Delta R_{\ell j} \geq 0.4$ for all jets with $E_T > 20$ GeV.

⁴In case of a jet faking a lepton, $W+$ jets can also give rise to dilepton events. Although we do not consider the possibility of such fakes, we expect the large M_{eff} cut to reduce this background significantly.

⁵Note that this K-factor has been obtained with a minimum p_T of 50 GeV for the jets whereas we will employ a cut of only 20 GeV. Based on the observation in Ref. [47], that in many cases the K-factor diminishes for processes with more hard jets, the actual K-factor for $t\bar{t} + 2$ jets might be lower than 1.28.

- The total energy deposit from all *hadronic activity* within a cone of $\Delta R \leq 0.2$ around the lepton axis should be ≤ 10 GeV.

Jet selection:

- Jets are formed with the help of PYCELL, the inbuilt cluster routine in PYTHIA. The minimum E_T of a jet is taken to be 20 GeV, and we also require $|\eta_j| < 2.5$.

We have approximated the detector resolution effects by smearing the energies (transverse momenta) with Gaussian functions. The different contributions to the resolution error have been added in quadrature.

- **Electron energy resolution:**

$$\frac{\sigma(E)}{E} = \frac{a}{\sqrt{E}} \oplus b \oplus \frac{c}{E}, \quad (9)$$

where

$$(a, b, c) = \begin{cases} (0.030 \text{ GeV}^{1/2}, 0.005, 0.2 \text{ GeV}), & |\eta| < 1.5, \\ (0.055 \text{ GeV}^{1/2}, 0.005, 0.6 \text{ GeV}), & 1.5 < |\eta| < 2.5. \end{cases} \quad (10)$$

- **Muon p_T resolution:**

$$\frac{\sigma(P_T)}{P_T} = \begin{cases} a, & p_T < 100 \text{ GeV}, \\ a + b \log \frac{p_T}{100 \text{ GeV}}, & p_T > 100 \text{ GeV}, \end{cases} \quad (11)$$

with

$$(a, b) = \begin{cases} (0.008, 0.037), & |\eta| < 1.5, \\ (0.020, 0.050), & 1.5 < |\eta| < 2.5. \end{cases} \quad (12)$$

- **Jet energy resolution:**

$$\frac{\sigma(E_T)}{E_T} = \frac{a}{\sqrt{E_T}}, \quad (13)$$

with $a = 0.5 \text{ GeV}^{1/2}$, the default value used in PYCELL.

Under realistic conditions, one would of course have to deal with aspects of misidentification of leptons.

An important cut will be imposed on the effective mass variable, defined to be the scalar sum of the transverse momenta of the isolated leptons and jets and the missing transverse energy,

$$M_{eff} = \sum p_T^{jets} + \sum p_T^{leptons} + \cancel{E}_T, \quad (14)$$

where the missing transverse energy is given by

$$\cancel{E}_T = \sqrt{\left(\sum p_x\right)^2 + \left(\sum p_y\right)^2}. \quad (15)$$

Here the sum goes over all the isolated leptons, the jets, as well as the ‘unclustered’ energy deposits. The energies of the ‘unclustered’ components, however, have not been smeared in this analysis.

In Fig. 1 we plot the distribution of the effective mass after the basic cuts (Cut-1) for dilepton events for the benchmark points BP-1 ($m_{q_H} \sim 400$ GeV), BP-2 ($m_{q_H} \sim 700$ GeV), BP-5 ($m_{q_H} \sim 1000$ GeV) and the SM background, dominantly from Drell-Yan and $t\bar{t}$ + jets. Recall that we have included appropriate K-factors for the latter process. The SM backgrounds are huge; however, the distributions peak around $2m_{q_H}$ for the signal and between M_Z and $2m_t$ for the SM background. It is clear that the production of heavy particles in the initial hard-scattering will lead to a high M_{eff} in most cases. Therefore, imposing the *effective mass cut*:

$$M_{eff} \geq 1 \text{ TeV} \quad (\text{Cut-2}), \quad (16)$$

will reduce the SM background substantially, although the distribution from SM processes with additional hard jets has a long tail towards larger values of M_{eff} . Note that the log-plot makes the differences between the curves look smaller than they actually are. Although this fixed cut also reduces the signal for the lighter $m_{q_H} \sim 400$ GeV from BP-1 by about half, the corresponding larger production cross-section makes up for this loss. In a more realistic analysis one would of course try to optimize the choice of the cut on M_{eff} , depending on the expected signal.

In addition to the effective mass cut from Eq. (16), we will also use the fact that we expect a peak in the invariant mass distribution of dileptons (M_{ll}) or four leptons (M_{4l}) near the mass of A_H . In our analysis, we will therefore impose the condition that the invariant mass should be in a *window around* M_{A_H}

$$M_{A_H} - 20 \text{ GeV} \leq M_{ll,4l} \leq M_{A_H} + 20 \text{ GeV} \quad (\text{Cut-3}). \quad (17)$$

As we will see, this condition will in particular help to reduce the background from leptons within the LHT model. Of course, in a realistic experimental analysis, where the mass of A_H is unknown, one would scan the whole range of invariant masses and impose such a window around some seed-mass M_{A_H} , thereby looking for an excess of the signal over the SM and LHT model backgrounds, which are almost flat except near the Z -mass. Moreover, this excess should stand out in this window, as compared to the adjoining bins.

Unfortunately, the need to implement such a cut in our analysis will not allow us to detect a heavy photon A_H with a mass very close to M_Z , since in that case the cut cannot free the peak from contamination by Z -production within the SM and in LHT cascades. In principle, by looking at the relative size of the branching fractions into charged leptons, including τ , and hadrons (jets), one might still be able to distinguish the A_H from the Z -boson. However, if we look at a heavy photon with $M_{A_H} = 92$ GeV, we get $R_{A_H} \equiv \text{BR}(A_H \rightarrow \text{quarks})/\text{BR}(A_H \rightarrow \text{all charged leptons}) = 6.27$, which is not much different from the corresponding ratio for the Z -boson, $R_Z = 6.92$. So the signature of A_H in this situation might be difficult to distinguish at the LHC. On the other hand, if the effective couplings of all charged leptons with the A_H are scaled up by a factor of two, as discussed above, we would get $R_{A_H} = 1.57$, which is quite different from the value for the Z -boson. Note that in this case $\text{BR}(A_H \rightarrow e^+e^-) + \text{BR}(A_H \rightarrow \mu^+\mu^-)$ changes from 7.58% for the original couplings to 22.66% for the rescaled leptonic couplings, i.e. it increases by a factor three and the required luminosity decreases correspondingly.

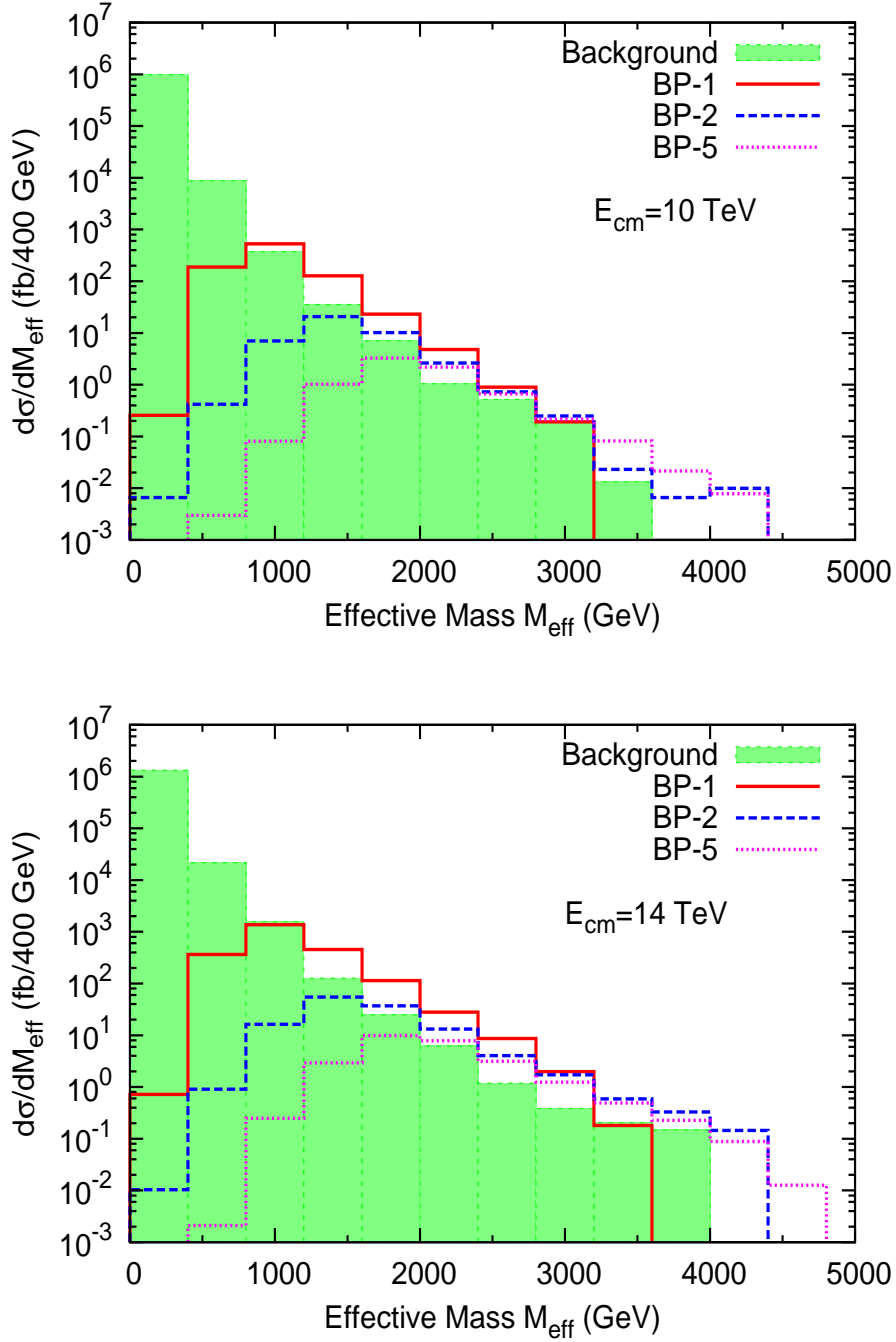


Figure 1: Effective mass distribution of dilepton events after the basic cuts (Cut-1) for BP-1 ($m_{qH} \sim 400$ GeV), BP-2 ($m_{qH} \sim 700$ GeV), BP-5 ($m_{qH} \sim 1000$ GeV) and the SM background, mostly Drell-Yan and $t\bar{t}$ + jets, at $\sqrt{s} = 10$ TeV (top panel) and $\sqrt{s} = 14$ TeV (bottom panel).

5 Results

5.1 Dilepton signal

5.1.1 LHC with $\sqrt{s} = 10$ TeV

In Table 3 we list, for the opposite sign same flavor (OSSF) dilepton signal ($l = e, \mu$), the cross-sections of the dominant SM background processes after the basic cuts (Cut-1) and the effective mass cut $M_{eff} > 1$ TeV (Cut-2) for the LHC running at $\sqrt{s} = 10$ TeV. We can see that the effective mass cut reduces all the SM dilepton backgrounds significantly, in particular from the Drell-Yan process via Z/γ^* , which is the overwhelming background after the basic cuts. After the cut on M_{eff} , $t\bar{t} + \text{jets}$ is the largest background due to the long tail in the effective mass distribution, see Fig. 1.⁶

Background	Cut-1 (fb)	Cut-2 (fb)
Z/γ^*	1247174	~ 0.00
$t\bar{t} + \text{jets}$	6278	84.03
$ZZ + \text{jets}$	546	5.76
$WW + \text{jets}$	946	9.58
$ZW + \text{jets}$	624	13.39
$tW + \text{jets}$	719	8.37
Total	1256287	121.13

Table 3: Dominant opposite sign same flavor dilepton ($l = e, \mu$) SM background cross-sections for $\sqrt{s} = 10$ TeV after the basic cuts (Cut-1) and after the cut $M_{eff} \geq 1$ TeV (Cut-2).

In our simulation of the Drell-Yan process with PYTHIA, out of 10^6 Monte-Carlo (MC) events, we did not see any dilepton event with $M_{eff} > 1$ TeV. Actually, in the simulation for the LHC running at 14 TeV, where the cross-section is higher and where we expect more events with larger M_{eff} , we did not get a single event with $M_{eff} > 1$ TeV out of 10^7 simulated Drell-Yan events. A larger MC sample would be needed to put a definite number on the cross-section after Cut-2. If we simply assume an upper bound of one event after Cut-2, which is probably much bigger than the correct number, this leads to an upper bound on the dilepton cross-section from Z/γ^* after Cut-2 of about 45 fb, i.e. quite sizeable compared to $t\bar{t}$. In the following we assume that we can neglect the SM background from Z/γ^* after the effective mass cut. In any case, after the Cut-3, i.e. that the dilepton invariant mass should be in a narrow window around M_{A_H} , see Eq. (17), a further reduction of the cross-section and number of dilepton events from Z/γ^* will occur anyway.

⁶We should note that in the simulation with ALPGEN a substantial number of events in $t\bar{t} + 4$ jets and $VV + 3$ jets ($V = W, Z$) pass the M_{eff} cut. We can therefore not exclude the possibility that the inclusion of more hard jets might increase the total background cross-section after Cut-2 by some amount. Such a simulation is beyond the scope of our present study. At least part of the effects of these hard jets is taken into account by the PYTHIA showering and MLM matching of the ALPGEN samples with the highest jet multiplicity.

In Fig. 2 we plot the invariant mass distributions of OSSF dileptons for all the benchmark points and the corresponding SM background after the basic cuts (Cut-1) and the M_{eff} cut (Cut-2). For BP-1, BP-2, BP-3 and BP-5, a peak emerges at the mass of A_H , in particular very clearly for BP-1 and BP-3. BP-1 has a large parton-level T-odd quark pair production cross-section because of the relatively small $m_{q_H} \sim 400$ GeV, compared to $m_{q_H} \sim 700$ GeV for BP-2. BP-3 has also $m_{q_H} \sim 700$ GeV, but a small value of $f = 500$ GeV. Therefore the T-odd quark production cross-section is strongly enhanced by electroweak contributions, as discussed earlier, see Table 2. Furthermore, the leptonic branching ratio for the light $M_{A_H} = 66$ GeV is also large, see Table 1, leading to more dilepton events. Note, however, that the ‘signal’ after Cut-2 also includes dileptons from within the LHT coming for instance from the decay via the Z -boson, leading to an enhancement in the peak at M_Z for BP-1 and BP-2 in Fig. 2. Since for BP-3 with $f = 500$ GeV the branching ratio $A_H \rightarrow l^+l^-$ is higher than for BP-1 and BP-2, the Z -peak is much smaller compared to the A_H -peak.

The total integrated luminosity at the LHC running at 10 TeV will probably be around 200 pb^{-1} . For this integrated luminosity, there will be 73 dilepton ‘signal’ events for BP-1 and 33 events for BP-3, compared to a SM background of 24 events. Note, however, that there will be only 8 dilepton events for BP-2 and 1.5 events for BP-5.

As mentioned in Section 2.2, the total decay width of A_H is only of the order of eV and therefore radiative corrections and detector effects will determine the observed width of the resonance peak in reality.

For BP-4 and BP-6 with $f = 1500$ GeV, the decay branching ratio $A_H \rightarrow l^+l^-$ is negligible compared to $A_H \rightarrow ZZ^{(*)}$, see Table 1, and therefore the four-lepton signal will be the relevant signature for discovery. Nevertheless, we get some dilepton events, in particular for BP-4, but the dilepton invariant mass distribution peaks at the Z -boson mass and not at M_{A_H} .

In order to reduce the SM background further, and also to eliminate the background from dileptons within the LHT which do not come from the decay $A_H \rightarrow l^+l^-$, we impose the additional constraint that the invariant mass of the dileptons should be in a window of ± 20 GeV around M_{A_H} (Cut-3), see Eq. (17). In Table 4 we give the cross-sections for OSSF dilepton events after the basic cuts (Cut-1) and after Cut-2 and Cut-3 for all the benchmark points for the LHC running at $\sqrt{s} = 10$ TeV. The total cross-section for the SM background after Cut-2 and Cut-3 is also given. We also list in Table 4 the number of signal and background events after Cut-2 and after Cut-3 for an integrated luminosity of 200 pb^{-1} .

We can see from Table 4 that with an integrated luminosity of 200 pb^{-1} , only BP-1 and BP-3 yield a clear signal over the SM background after Cut-2. The Cut-3 then reduces the SM background and the dilepton background from within the LHT model almost completely, with $S_3/B_3 = 15.7$ for BP-1 and $S_3/B_3 = 5.7$ for BP-3 with more than 10 signal events for both benchmark points. Although the high $M_{eff} \geq 1$ TeV cut (Cut-2) reduces the signal for BP-1 with a low mass $m_{q_H} = 400$ GeV by about a factor two, the larger production cross-section compensates for that. Therefore, at least for BP-1 and BP-3, one expects a clear dilepton signal from the decay of the A_H in the LHT with T-parity violation at the early stage of the LHC run with low center of mass energy and modest luminosity. With the predicted number of signal events after Cut-3, it will presumably also be possible to reconstruct the mass of A_H and determine the symmetry breaking scale f .

If we demand that we have at least 10 signal events, BP-2 yields not enough events

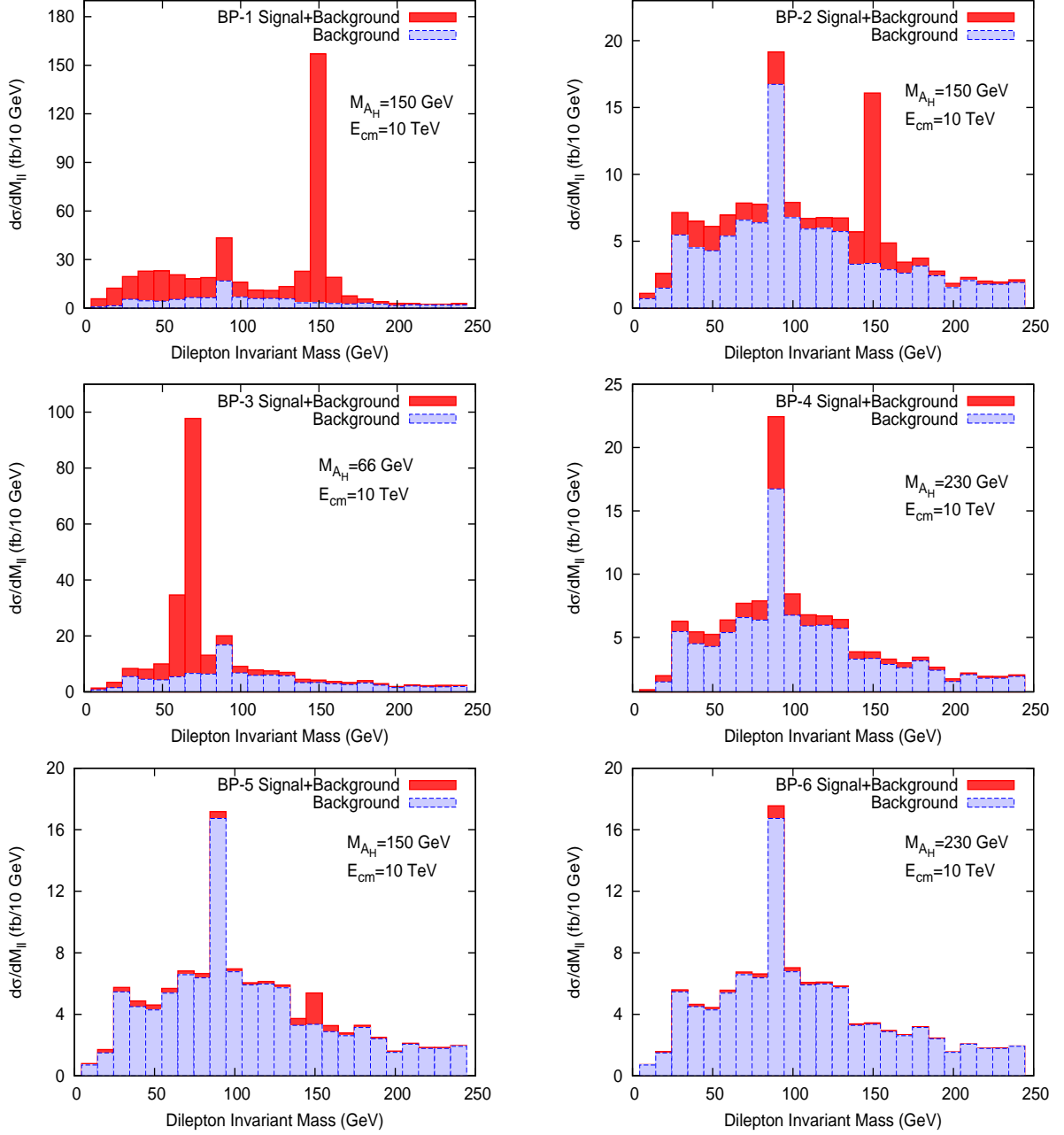


Figure 2: Invariant mass distribution of OSSF dilepton pairs ($l = e, \mu$) for $\sqrt{s} = 10$ TeV after the basic cuts (Cut-1) and the effective mass cut $M_{eff} \geq 1$ TeV (Cut-2) for all the benchmark points, with the corresponding SM background. Note that the ‘signal’ also includes dileptons within the LHT not coming from A_H , but, for instance through the decay of the Z -boson. This is in particular the case for BP-4 and BP-6 where we do not expect any dileptons from A_H . For an integrated luminosity of 200 pb^{-1} there are 73 signal events for BP-1 and 33 events for BP-3, but only 8 signal events for BP-2 and 1.5 events for BP-5, compared to 24 events from the SM background. See Table 4 for more details.

	Cut-1 [S] (fb)	Cut-2 [S] (fb)	Cut-2 [BG] (fb)	S_2	B_2	Cut-3 [S] (fb)	Cut-3 [BG] (fb)	S_3	B_3
BP-1	871.5	367.0	121.1	73.4	24.2	196.7	12.4	39.3	2.5
BP-2	41.9	39.8	121.1	8.0	24.2	18.2	12.4	3.6	2.5
BP-3	175.2	168.1	121.1	33.6	24.2	132.9	23.3	26.6	4.7
BP-4	21.9	21.3	121.1	4.3	24.2	0.5	7.2	0.1	1.4
BP-5	7.6	7.6	121.1	1.5	24.2	3.1	12.4	0.6	2.5
BP-6	3.5	3.5	121.1	0.1	24.2	0.1	7.2	0.02	1.4

Table 4: OSSF dilepton signal (S) from all T-odd quark-pair production processes and total SM background (BG) cross-sections at the LHC with $\sqrt{s} = 10$ TeV after the different cuts described in the text. The number of signal and background events after Cut-2 with an integrated luminosity of 200 pb^{-1} are also given as S_2 and B_2 , respectively. The corresponding numbers after Cut-3 are denoted by S_3 and B_3 .

with an integrated luminosity of 200 pb^{-1} , in particular after Cut-3. Furthermore, with this luminosity there will be almost no dilepton events for BP-5, already after Cut-2, because of the small production cross-section for $m_{q_H} \sim 1$ TeV. Also the branching ratio of A_H into dileptons is small for this benchmark point, since $f = 1$ TeV.

Note that the BP-4 with $M_{A_H} = 230$ GeV yields about half the dilepton events of BP-2 for the same mass $m_{q_H} \sim 700$ GeV of the heavy T-odd quarks. However, these dileptons for BP-4 are not coming from the decay $A_H \rightarrow l^+l^-$, but from other sources, mostly the Z -boson, as mentioned above. In Table 4 this is visible after imposing the Cut-3 which almost completely removes all dilepton events for BP-4, whereas about half the dilepton events survive for BP-2. For BP-6 there are essentially no dilepton events for 200 pb^{-1} . As for BP-4, we expect for this benchmark point, which has $f = 1500$ GeV and $M_{A_H} = 230$ GeV, the four-lepton mode to be relevant for discovery.

We should caution the reader about the numbers given in Table 4 for the SM background cross-sections and the number of BG events after Cut-2 and in particular after Cut-3. The total number of MC events in the OSSF channel we simulated (including all possible processes) is 350987 after Cut-1. After the cut on M_{eff} (Cut-2), we have 4296 events in our MC sample and after Cut-3 there remain 644 MC events in the window of ± 20 GeV around the A_H mass (for the case $M_{A_H} = 66$ GeV). Therefore, there is an intrinsic uncertainty of about 4% on the numbers for B_3 given in the Table 4. A much larger MC simulation to pin down these numbers more precisely is beyond the scope of the present work. Note, however, that we have enough simulated events for the signal. For instance, for BP-2, we have 12041 MC events after Cut-2 and 5501 MC events after Cut-3.

5.1.2 LHC with $\sqrt{s} = 14$ TeV

In Table 5 we list, for the opposite sign same flavor (OSSF) dilepton signal ($l = e, \mu$), the cross-sections of the dominant SM background processes after the basic cuts (Cut-1) and the effective mass cut $M_{eff} > 1$ TeV (Cut-2) for the LHC running at $\sqrt{s} = 14$ TeV. As

for 10 TeV, we can see that the effective mass cut reduces all the SM dilepton backgrounds significantly, in particular from the Drell-Yan process via Z/γ^* which is the main background after the basic cuts. Again, after the cut on M_{eff} , $t\bar{t}$ is the largest background due to the long tail in the effective mass distribution, see Fig. 1. As noted in the previous subsection, in our simulation of the Drell-Yan process with PYTHIA, we did not see any dilepton event with $M_{eff} > 1$ TeV out of 10^7 MC events. There were 30048 OSSF dilepton MC events which passed the basics cuts. If we would simply assume an upper bound of one event after the Cut-2, which might be way off the correct number, this would lead to an upper bound on the dilepton cross-section from Z/γ^* after Cut-2 of about 57 fb, i.e. again quite sizeable compared to $t\bar{t}$. In the following we assume again that we can neglect the SM background from Z/γ^* after Cut-2.

Background	Cut-1 (fb)	Cut-2 (fb)
Z/γ^*	1711746	~ 0.00
$t\bar{t} + \text{jets}$	13854	344.33
$ZZ + \text{jets}$	827	13.82
$WW + \text{jets}$	1385	30.17
$ZW + \text{jets}$	951	43.40
$tW + \text{jets}$	1604	41.89
Total	1730366	473.61

Table 5: Same as Table 3 for $\sqrt{s} = 14$ TeV.

In Fig. 3 we plot the invariant mass distributions of OSSF dileptons for all the benchmark points and the corresponding SM background after the basic cuts (Cut-1) and the cut on M_{eff} (Cut-2). Again for BP-1, BP-2, BP-3 and BP-5, a peak emerges at the mass of A_H , in particular very clearly for BP-1, BP-2 and BP-3. With an integrated luminosity of 30 fb^{-1} , there are 36088 signal events for BP-1, 3723 events for BP-2 and 2135 events for BP-3, compared to 14208 SM background events. Again, for BP-1 and BP-2 we have a non-negligible amount of dilepton background from within the LHT, in particular from the decays via the Z -boson, as can be clearly seen in the Fig. 3.

As mentioned before, for BP-4 and BP-6 with $f = 1500$ GeV, the decay branching ratio $A_H \rightarrow l^+l^-$ is negligible compared to $A_H \rightarrow ZZ^{(*)}$, see Table 1, and therefore the four-lepton signal will be the relevant signature for discovery. Nevertheless, we get many dilepton events even for these two benchmark points, but there is a peak at the Z -boson mass and not at M_{A_H} .

In order to reduce the SM background further, but also to eliminate the background from dileptons within the LHT which do not come from the decay $A_H \rightarrow l^+l^-$, we impose again the additional constraint that the invariant mass of the dileptons should be in a window around M_{A_H} (Cut-3), see Eq. (17). In Table 6 we give the cross-sections for OSSF dilepton events after the basic cuts (Cut-1) and after Cut-2 and Cut-3 for all the benchmark points for the LHC running at $\sqrt{s} = 14$ TeV. The total cross-section for the SM background after Cut-2 and Cut-3 is also given. We also list in Table 6 the number of signal and background

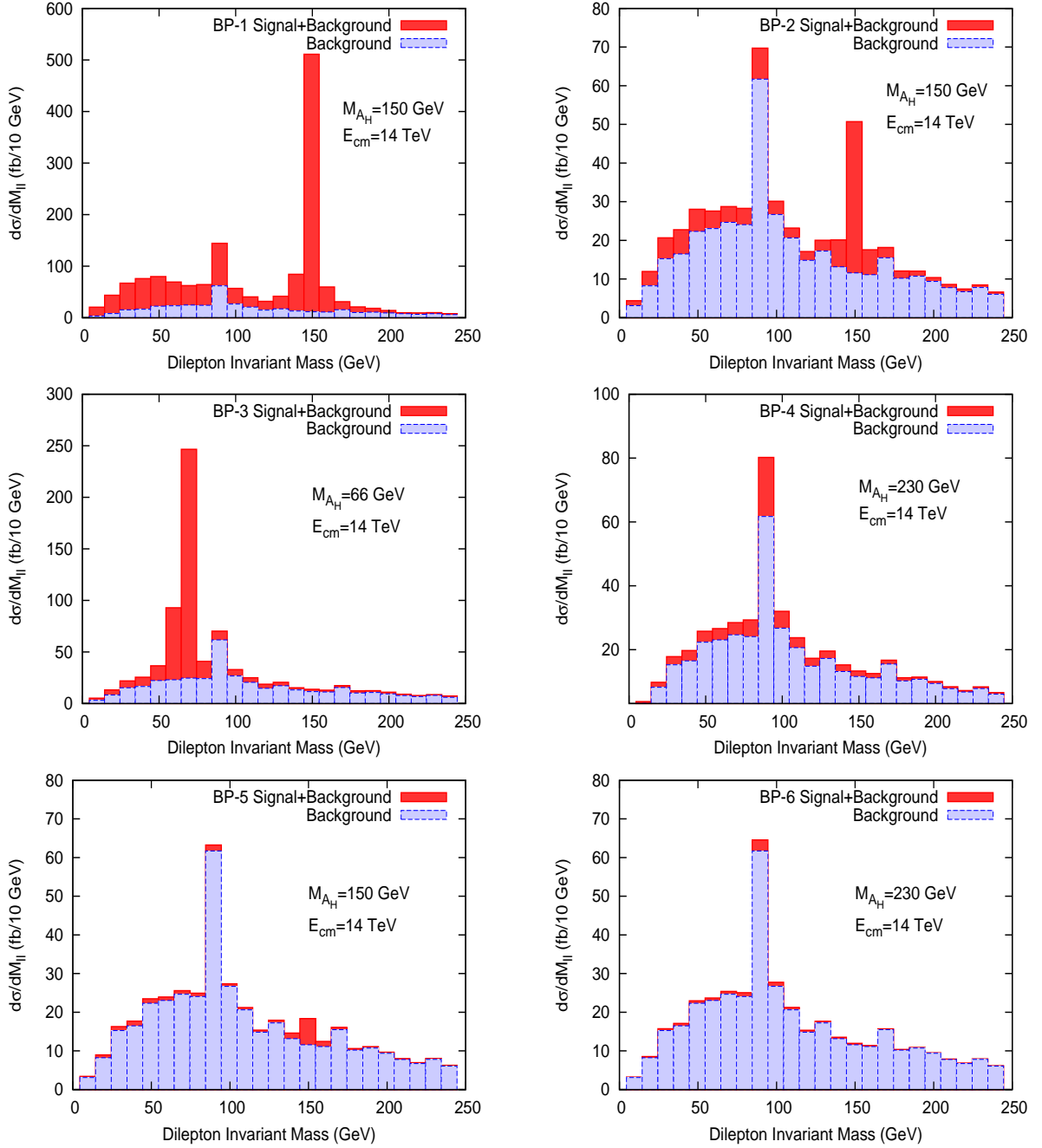


Figure 3: Same as Fig. 2 for $\sqrt{s} = 14$ TeV.

events after Cut-2 and after Cut-3 for an integrated luminosity of 30 fb^{-1} .

The qualitative features of the benchmark points for the LHC running at $\sqrt{s} = 14$ TeV are very similar to the case of $\sqrt{s} = 10$ TeV, but now we have higher event rates. First of all, after the Cut-2, all the signal and background cross-sections are about a factor of three bigger, see Tables 4 and 6. Furthermore, we assume that we have now much more integrated

luminosity, 30 fb^{-1} compared to 200 pb^{-1} earlier. The Cut-2 again removes about half of the signal events for BP-1. For all benchmark points, we now get more than 10 signal events even after Cut-3 and also the number of background events is much larger than 100. It makes therefore sense to consider the signal significance by looking at S/\sqrt{B} which is also given in Table 6 for the number of events after Cut-3.

	Cut-1 [S] (fb)	Cut-2 [S] (fb)	Cut-2 [BG] (fb)	S_2	B_2	Cut-3 [S] (fb)	Cut-3 [BG] (fb)	S_3	B_3	$S_3/\sqrt{B_3}$
BP-1	2341.8	1202.9	473.6	36088	14208	642.9	50.3	19286	1508	496.6
BP-2	129.1	124.1	473.6	3723	14208	55.5	50.3	1665	1508	42.9
BP-3	428.9	413.3	473.6	12398	14208	322.9	95.8	9686	2873	180.7
BP-4	72.7	71.2	473.6	2135	14208	1.9	27.0	56	809	2.0
BP-5	26.1	26.0	473.6	781	14208	10.3	50.3	308	1508	7.9
BP-6	13.4	13.4	473.6	401	14208	0.4	27.0	11	809	0.4

Table 6: Same as Table 4 for $\sqrt{s} = 14 \text{ TeV}$ and an integrated luminosity of 30 fb^{-1} .

Looking at the significance, we can now better see the importance of imposing the Cut-3, i.e. the dilepton invariant mass should be in a window of $\pm 20 \text{ GeV}$ around M_{A_H} . For instance, BP-4 has 2135 dilepton events for 30 fb^{-1} , but they are not coming from the decay $A_H \rightarrow l^+l^-$ as mentioned earlier, but instead from Z -decays. After Cut-2 we get a large apparent statistical significance of $S_2/\sqrt{B_2} = 17.9$ (note that $\sqrt{B_2} = 119.2$), but the huge reduction in the number of events after Cut-3, from 2135 down to 56 events, tells us that these dileptons are not coming from the decay of A_H , instead they come from an almost flat background. Of course, this can be clearly seen by looking at the plot of the dilepton invariant mass distribution in Fig. 3. On the other hand, the Cut-3 removes only about one third of the signal events for BP-3 and about half the events for BP-1, BP-2 and BP-5. This indicates the presence of a peak around M_{A_H} for these benchmark points, see Fig. 3. But note that for BP-4 even after Cut-3, we still have $S_3/\sqrt{B_3} = 2.0$, but, of course, there will be no peak in the dilepton distribution around A_H . Even for BP-6 we get after Cut-2 a signal of $S_2/\sqrt{B_2} = 3.4$, but again they are not from the dilepton decay of the A_H , as can be seen after Cut-3 is applied where we get $S_3/\sqrt{B_3} = 0.4$.

We have seen in the previous Section 5.1.1 for the LHC running at $\sqrt{s} = 10 \text{ TeV}$ and with 200 pb^{-1} integrated luminosity that we had a clear dilepton signal over the SM background for BP-1 and BP-3.

It is obvious from the last column in Table 6 that with a center of mass energy of 14 TeV and an integrated luminosity of 30 fb^{-1} , we can now also cover BP-2 and BP-5. That means it will be possible at these benchmark points to reconstruct the peak of A_H in the dilepton invariant mass distribution and to determine the mass M_{A_H} and the scale f . In particular with an integrated luminosity of 11.9 fb^{-1} , it will be possible to get 5σ statistical significance for BP-5 after Cut-3. As a reminder, BP-5 has a rather heavy T-odd quark mass of $m_{q_H} \sim 1 \text{ TeV}$. Furthermore we have chosen the difficult intermediate region with $f = 1 \text{ TeV}$, where the dilepton mode is not dominant. For lower f , the discovery will be

even easier for the same m_{qH} or, conversely, for lower f , we get a larger reach in m_{qH} , if we demand a 5σ signal with 30 fb^{-1} .

Again we should caution the reader about the numbers given in Table 6 for the SM background cross-sections and the number of BG events after Cut-2 and in particular after Cut-3, because of the limited statistics in the Monte-Carlo simulation. The total number of MC events in the OSSF channel we simulated (including all possible processes) is 139429 after Cut-1. After the cut on M_{eff} (Cut-2), we have 4170 events in our MC sample and after Cut-3 there remain 730 MC events in the window of $\pm 20 \text{ GeV}$ around the A_H mass (for the case $M_{A_H} = 66 \text{ GeV}$). Therefore, there is an intrinsic uncertainty of about 4% on the numbers for B_3 given in the Table 6 and correspondingly about 2% uncertainty on the significance $S_3/\sqrt{B_3}$. In particular, the required luminosity for a 5σ statistical significance for BP-5 should be taken with a grain of salt. A much larger MC simulation to pin down these numbers more precisely is again beyond the scope of the present work. Note, however, that we have enough simulated events for the signal. For instance, for BP-5, we have 12365 MC events after Cut-2 and 4880 MC events after Cut-3.

5.2 Four-lepton signal

5.2.1 LHC with $\sqrt{s} = 10 \text{ TeV}$

The biggest SM background for the four-lepton signal, as defined in Section 4.1, arises from the production of $ZZ + \text{jets}$ and the subsequent fully leptonic decays.⁷ For the LHC running at $\sqrt{s} = 10 \text{ TeV}$, the corresponding cross-section after the basic cuts (Cut-1) is 13.78 fb . It is drastically reduced to 0.14 fb by the cut on the effective mass $M_{eff} \geq 1 \text{ TeV}$ (Cut-2). The second largest SM background is from $t\bar{t} + \text{jets}$, but after the basic cuts and the requirement that at least two OSSF leptons among the total four have an invariant mass in a window of $\pm 20 \text{ GeV}$ around M_Z , it is only 0.53 fb and it is completely removed by the effective mass cut.

In Table 7 we list for all the benchmark points, except BP-3, the cross-sections for the four-lepton signal for the LHC running at a center of mass energy of 10 TeV , successively after the basic cuts (Cut-1), Cut-2 on the effective mass and Cut-3, i.e. the condition that the four-lepton invariant mass should be in a window of $\pm 20 \text{ GeV}$ around the mass of A_H , see Eq. (17). The total SM background after Cut-2 and Cut-3 is also given. Note that for BP-3 with $f = 500 \text{ GeV}$, the BR of A_H into $ZZ^{(*)}$ is essentially zero, see Table 1, and therefore we have not included that benchmark point in the table.

Unfortunately, although the four-lepton signal cross-sections are larger than the SM background after Cut-2 for all the benchmark points considered in the table, there will be always less than 10 signal events for an integrated luminosity of 200 pb^{-1} . Therefore we will not be able to see a clear A_H mass peak in the early stages of the LHC run.

5.2.2 LHC with $\sqrt{s} = 14 \text{ TeV}$

The biggest SM background for the four-lepton signal comes again from $ZZ + \text{jets}$ production. For the LHC running at $\sqrt{s} = 14 \text{ TeV}$, the corresponding cross-section after the basic

⁷For details on a method to normalize the production rate of ZZ from data see Ref. [50].

	Cut-1 S (fb)	Cut-2 S (fb)	Cut-2 BG (fb)	Cut-3 S (fb)	Cut-3 BG (fb)
BP-1	21.70	6.45	0.14	1.53	0.003
BP-2	1.21	1.07	0.14	0.19	0.003
BP-4	1.34	1.26	0.14	0.33	0.010
BP-5	0.23	0.23	0.14	0.02	0.003
BP-6	0.18	0.18	0.14	0.04	0.010

Table 7: Four-lepton signal cross-sections (S) for $\sqrt{s} = 10$ TeV after the basic cuts (Cut-1), after Cut-2 and after Cut-3. For BP-3 there is no signal. The total SM background (BG) cross-section (mostly from ZZ) after Cut-2 and Cut-3 is also given. Note that we always demand that among the four leptons, there is always at least one OSSF lepton pair with its invariant mass being around ± 20 GeV of M_Z .

cuts (Cut-1) is 18.79 fb. It is drastically reduced to 0.40 fb by the cut on the effective mass $M_{eff} \geq 1$ TeV. The second largest SM background is from $t\bar{t} + \text{jets}$. After the basic cuts and the requirement that at least two OSSF leptons among the total four have an invariant mass around M_Z , it is 0.26 fb, but it is again completely removed by the effective mass cut.

In Fig. 4 we show the four-lepton invariant mass distributions for all the benchmark points, except BP-3, and the corresponding SM background for the LHC running at $\sqrt{s} = 14$ TeV after the basics cuts (Cut-1) and the cut of M_{eff} (Cut-2).

As can be seen from Fig. 4, after the effective mass cut (Cut-2) the signal is larger than the SM background, except for BP-5 and BP-6. But for all benchmark points a clear peak emerges at the mass of A_H . Note that we do not observe any four-lepton events with an invariant mass of less than 100 GeV, which reflects the fact that we demand at least one OSSF lepton pair to have an invariant mass around M_Z .

In Table 8 we list for all the benchmark points, except BP-3, the cross-sections for the four-lepton signal for the LHC running at a center of mass energy of 14 TeV after the basic cuts (Cut-1), after Cut-2 on the effective mass and after Cut-3. The total SM background after Cut-2 and Cut-3 is also given. In addition, we give the number of events for an integrated luminosity of 30 fb^{-1} after Cut-2 and after Cut-3.

We can see from the table that Cut-2, as for the dilepton signal, removes about half of the four-lepton events for BP-1, but this is compensated by the large parton-level cross section for $m_{q_H} \sim 400$ GeV. The Cut-3 reduces the signal by a factor of six for BP-2, by a factor of four for BP-4 and by a factor of three for BP-1.

It is obvious that with essentially no background, we have a very clear signal and many events after Cut-3 for BP-1 and BP-4 with 30 fb^{-1} of integrated luminosity. This should allow the reconstruction of the peak of the A_H boson and the determination of the mass M_{A_H} . For BP-2 we have about 14 events after Cut-3, therefore the reconstruction of the peak might not be so precise.

Recall that from the dilepton signature, we had a significant signal over the background for BP-1 and BP-3 at $\sqrt{s} = 10$ TeV and with 200 pb^{-1} of integrated luminosity. In addition,

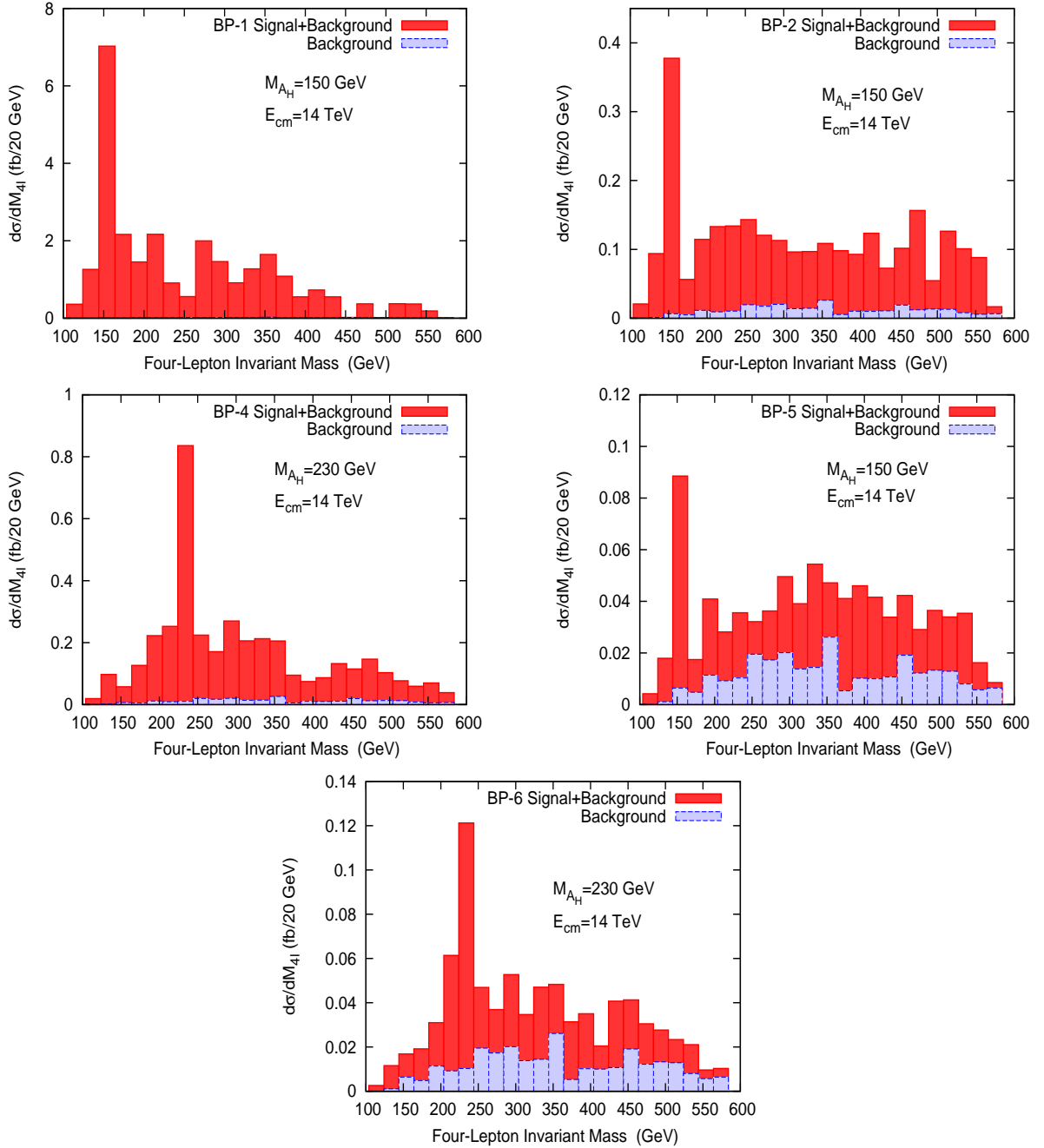


Figure 4: Four-lepton invariant mass distribution for all the benchmark points, except BP-3, where we do not expect any signal, after the basic cuts (Cut-1) and after the cut on $M_{eff} \geq 1$ TeV (Cut-2) for $\sqrt{s} = 14$ TeV.

at $\sqrt{s} = 14$ TeV and with 30 fb^{-1} , we could also cover BP-2 and BP-5. Now, with four-lepton events, we get a very clear signal after Cut-3 for BP-4 (34 events compared to about 1 background event) and, for an integrated luminosity of about 59 fb^{-1} , we would get at least

	Cut-1 [S] (fb)	Cut-2 [S] (fb)	Cut-2 [BG] (fb)	S_2	B_2	Cut-3 [S] (fb)	Cut-3 [BG] (fb)	S_3	B_3
BP-1	58.85	28.80	0.40	864.0	12	9.18	0.01	275.4	0.3
BP-2	3.12	2.89	0.40	86.7	12	0.47	0.01	14.1	0.3
BP-4	4.25	4.02	0.40	120.6	12	1.12	0.03	33.6	0.9
BP-5	0.79	0.79	0.40	23.7	12	0.10	0.01	3.0	0.3
BP-6	0.67	0.66	0.40	19.8	12	0.17	0.03	5.1	0.9

Table 8: Same as Table 7 for $\sqrt{s} = 14$ TeV. The number of signal and background events after Cut-2 with an integrated luminosity of 30 fb^{-1} are also given as S_2 and B_2 , respectively. The corresponding numbers after Cut-3 are denoted by S_3 and B_3 .

10 signal events even for BP-6, with around 2 background events. Both of these benchmark points have $f = 1500$ GeV and the branching fraction $A_H \rightarrow ZZ$ is 22.5% and thus it is enhanced compared to BP-1 and BP-2, where for $f = 1000$ GeV it is only about 11%, see Table 1. This allows us to use the four-lepton signal for discovery for BP-4 and, maybe, BP-6.

Of course, it would be a convincing cross-check on the LHT model with T-parity violation, if one could see the A_H peak in the dilepton and in the four-lepton channel at the same mass. At least for BP-1 and BP-2 this will be possible with the LHC running at 14 TeV and with 30 fb^{-1} . For BP-5, we would need 100 fb^{-1} to get 10 four-lepton signal events after Cut-3. Note that other New Physics models which have such a Z' -type boson like the A_H might lead to a different pattern in the invariant mass distributions or the relative number of events in the dilepton and four-lepton channels might be very different from the ones in the LHT.

As suggested in Ref. [21], looking at the angular distributions of the two lepton pairs coming from ZZ -decays, one might be able to determine whether the decay $A_H \rightarrow ZZ$ is really described by a vertex which originates from the WZW-term. At least for BP-1 with 275 four-lepton events after Cut-3, such an analysis seems to be feasible.

6 Summary and Conclusions

In this work we have analyzed dilepton and four-lepton events (here lepton means electron or muon) at the LHC originating from the decay of the heavy photon A_H in the Littlest Higgs model with T-parity violation. These decays of A_H , assumed to be the lightest T-odd particle, are induced by T-violating couplings from the Wess-Zumino-Witten anomaly term.

Since the WZW term reproduces, within the EFT, the chiral anomalies in the UV completion of the LHT, its prefactor $N/48\pi^2$ corresponds to a one-loop effect. Furthermore, because of gauge invariance, the actual coupling of A_H to SM gauge bosons has an additional suppression factor of v^2/f^2 . For larger masses $M_{A_H} > 150$ GeV, A_H predominantly decays into $WW^{(*)}$ and $ZZ^{(*)}$. On the other hand, for smaller masses, loop-induced decays into SM fermions are possible. The corresponding one-loop diagrams in the EFT are, however, UV divergent and one needs counterterms with *a priori* unknown coefficients. Following

Ref. [20] these coefficients have been fixed by naive dimensional analysis. The couplings of A_H to SM fermions are then effectively of the size of two-loop effects.

Due to the tiny coupling of A_H to SM particles, its direct production at e^+e^- or hadron colliders only has a cross-section of the order of 10^{-6} pb. On the other hand, the production of the other T-odd particles is not affected by the presence of the WZW term. Therefore, these particles are still pair-produced and cascade decay down to A_H by the T-conserving interactions in the LHT and finally the two A_H 's decay promptly in the detector. The crucial observation, already made in Ref. [21], is that summing all production processes of heavy T-odd quark pairs leads to a sizeable cross-section at the LHC, of the order of several pb, and this corresponds to a lower bound on the production cross-section of A_H pairs.

We have studied the dilepton and four-lepton signals for six benchmark points, see Table 2, which have different values for the heavy quark mass $m_{q_H} \sim 400, 700, 1000$ GeV and different values for the mass of the heavy photon $M_{A_H} = 66, 150, 230$ GeV ($f = 500, 1000, 1500$ GeV). The values of the heavy quark mass essentially determine the parton-level pair-production cross-section via strong interaction processes, although the effects of electroweak contributions from t -channel exchanges of A_H and Z_H can be very important and even dominate for low values of f , i.e. light A_H and Z_H . On the other hand, the mass of A_H determines the expected signal because of the different branching ratios into leptons or ZZ , see Table 1. For low and intermediate masses of A_H , the dilepton decays are sizeable, whereas for $M_{A_H} = 230$ GeV the decay into ZZ and then into four-leptons is relevant.

We have studied the case of the LHC running at a center of mass energy of $\sqrt{s} = 10$ TeV with a modest integrated luminosity of 200 pb^{-1} and the case of $\sqrt{s} = 14$ TeV with an integrated luminosity of 30 fb^{-1} .

In order to reduce the SM background from Z/γ^* and $t\bar{t} + \text{jets}$ for the dilepton signal and from $ZZ + \text{jets}$ for the four-lepton signal, we have imposed a large cut on the effective mass of the events of $M_{eff} > 1$ TeV, since in general M_{eff} approximately peaks at the sum of the masses of the initially produced particles. Essentially, this cut removes a considerable fraction of the SM backgrounds, except for processes with multiple additional hard jets, which have a long tail in the effective mass distribution (see Figure 1). On the other hand, there are many sources of leptons in the decay cascades leading to A_H and in general we also get many events with leptons which do not originate from the decay of A_H . We have reduced the corresponding background from within the LHT by imposing the condition that the invariant mass of dileptons or four leptons should lie in a window of ± 20 GeV around M_{A_H} .

For the *dilepton signal*, the main conclusion is that for regions of the parameter space where either the T-odd quarks are relatively light, $m_{q_H} \sim 400$ GeV (BP-1 with $f = 1000$ GeV) or the scale f is rather low, $f = 500$ GeV (BP-3 with $m_{q_H} \sim 700$ GeV), we get after all the cuts a clear signal above the background for the early run of the LHC with center of mass energy of 10 TeV and integrated luminosity of 200 pb^{-1} . More details can be found in Table 4. For the LHC with $\sqrt{s} = 14$ TeV and 30 fb^{-1} luminosity, also BP-2 ($m_{q_H} \sim 700$ GeV, $M_{A_H} = 150$ GeV) and BP-5 ($m_{q_H} \sim 1000$ GeV, $M_{A_H} = 150$ GeV) yield a significant signal with $S/\sqrt{B} = 42.9$ for the former and $S/\sqrt{B} = 7.9$ for the latter benchmark point, see Table 6 for details.

The *four-lepton channel* is very clean and the signal cross-sections are larger than the SM backgrounds after all the cuts, with the exception of BP-3 with small $f = 500$ GeV,

where we do not expect a four-lepton signal. Unfortunately, for the LHC running at 10 TeV and with 200 pb^{-1} of integrated luminosity, we always get less than 10 signal events. For $\sqrt{s} = 14 \text{ TeV}$ and 30 fb^{-1} , the background is again negligible (< 0.9 events) and we can easily cover again BP-1 and BP-2. In addition, we now also get a clear signal for BP-4 ($m_{q_H} \sim 700 \text{ GeV}$, $M_{A_H} = 230 \text{ GeV}$). We would need 59 fb^{-1} to get 10 signal events for BP-6 ($m_{q_H} \sim 1000 \text{ GeV}$, $M_{A_H} = 230 \text{ GeV}$). Note that these BP's with large $f = 1500 \text{ GeV}$ can only be covered in the four-lepton channel. Details can be found in Table 8.

Therefore, with the LHC running at 14 TeV and an integrated luminosity of 30 fb^{-1} , we can cover with the dilepton and / or the four-lepton signal a large part of the typical parameter space of the LHT with values of f up to 1500 GeV and with T-odd quark masses up to about 1000 GeV. In general, a clear peak emerges at M_{A_H} , if one plots the invariant mass distributions for dileptons, see Fig. 2 for the LHC running at 10 TeV, and Fig. 3 for $\sqrt{s} = 14 \text{ TeV}$. The four-lepton invariant mass distribution for the LHC at 14 TeV is shown in Fig. 4. For all the studied benchmark points we have enough signal events after all the cuts, therefore it should be easy to reconstruct the mass peak of A_H , maybe with the exception of BP-6.

Note that the reconstruction of the peak and the measurement of M_{A_H} directly determines the symmetry breaking scale f in the LHT, which is one of the fundamental parameters of any Little Higgs model. Together with the M_{eff} distribution which peaks around $2m_{q_H}$, this would then allow a rough determination of the parameter κ_q as well.

Of course, it would also be an important cross-check on the LHT model with T-parity violation, if we could see the A_H peak in both the dilepton and the four-lepton channel at the same mass. This, including the ratio of events in the two channels, distinguishes the case of A_H in the LHT from other models of New Physics, like most Z' models. At least for benchmark points with intermediate values of $f = 1000 \text{ GeV}$, which yield both enough dilepton and four-lepton events, this could be achieved. For BP-1 and BP-2 this will be possible for the LHC running at 14 TeV and with 30 fb^{-1} . For BP-5 we would need 100 fb^{-1} to get 10 four-lepton events (with essentially very low background).

Finally, we should stress again that the WZW term offers a unique window into the UV completion of the LHT. The parameter N determines the total decay width of A_H , but since the width is only a few eV, it cannot be measured experimentally. Furthermore, in the decay branching ratios, the factor N drops out. On the other hand, the finite parts of the counterterms needed to renormalize the one-loop diagrams in the EFT are determined by the underlying theory. In principle, measuring the branching ratios of A_H would therefore yield information on the more fundamental theory. As briefly discussed, if these branching ratios of the decays into leptons or quarks differ substantially from those of the Z -boson, one might even be able to see a signal from A_H with a mass close to M_Z .

Note added. After this manuscript was first submitted, the LHC schedule was revised, targetting a run at 7 TeV with about $1 - 2 \text{ fb}^{-1}$ luminosity, followed by a direct upgrade to 14 TeV. Since the 14 TeV run maximizes our reach in the parameter space, we have presented the results corresponding to this energy in detail. However, we have also retained the results for 10 TeV.

Acknowledgments

S.M. would like to thank Sanjoy Biswas and Nishita Desai for many useful discussions and technical help. We also thank V. Ravindran for valuable discussions and Bruce Mellado for an important comment on the manuscript. This work was partially supported by funding available from the Department of Atomic Energy, Government of India, for the Regional Centre for Accelerator-based Particle Physics (RECAPP), Harish-Chandra Research Institute. Computational work for this study was partially carried out at the cluster computing facility in the Harish-Chandra Research Institute (<http://cluster.hri.res.in>).

References

- [1] N. Arkani-Hamed, A. G. Cohen and H. Georgi, Phys. Lett. B **513**, 232 (2001); N. Arkani-Hamed, A. G. Cohen, T. Gregoire and J. G. Wacker, JHEP **0208**, 020 (2002).
- [2] For reviews, see M. Schmaltz and D. Tucker-Smith, Ann. Rev. Nucl. Part. Sci. **55**, 229 (2005); M. Perelstein, Prog. Part. Nucl. Phys. **58**, 247 (2007); M. C. Chen, Mod. Phys. Lett. A **21**, 621 (2006); E. Accomando *et al.*, hep-ph/0608079, Chapter 7.
- [3] R. Barbieri and A. Strumia, hep-ph/0007265; Phys. Lett. B **462**, 144 (1999).
- [4] S. R. Coleman and E. Weinberg, Phys. Rev. D **7**, 1888 (1973).
- [5] N. Arkani-Hamed, A. G. Cohen, E. Katz and A. E. Nelson, JHEP **0207**, 034 (2002).
- [6] C. Csaki *et al.*, Phys. Rev. D **67**, 115002 (2003); J. L. Hewett, F. J. Petriello and T. G. Rizzo, JHEP **0310**, 062 (2003); C. Csaki *et al.*, Phys. Rev. D **68**, 035009 (2003); M. Perelstein, M. E. Peskin and A. Pierce, Phys. Rev. D **69**, 075002 (2004); M. C. Chen and S. Dawson, Phys. Rev. D **70**, 015003 (2004); W. Kilian and J. Reuter, Phys. Rev. D **70**, 015004 (2004); G. Marandella, C. Schappacher and A. Strumia, Phys. Rev. D **72**, 035014 (2005).
- [7] H. C. Cheng and I. Low, JHEP **0309**, 051 (2003); JHEP **0408**, 061 (2004).
- [8] I. Low, JHEP **0410**, 067 (2004).
- [9] J. Hubisz and P. Meade, Phys. Rev. D **71**, 035016 (2005).
- [10] J. Hubisz, P. Meade, A. Noble and M. Perelstein, JHEP **0601**, 135 (2006).
- [11] C. R. Chen, K. Tobe and C. P. Yuan, Phys. Lett. B **640**, 263 (2006).
- [12] M. Asano, S. Matsumoto, N. Okada and Y. Okada, Phys. Rev. D **75**, 063506 (2007).
- [13] R. S. Hundi, B. Mukhopadhyaya and A. Nyffeler, Phys. Lett. B **649**, 280 (2007).
- [14] A. Birkedal, A. Noble, M. Perelstein and A. Spray, Phys. Rev. D **74**, 035002 (2006); C. S. Chen, K. Cheung and T. C. Yuan, Phys. Lett. B **644**, 158 (2007).

- [15] C. T. Hill and R. J. Hill, Phys. Rev. D **75**, 115009 (2007); Phys. Rev. D **76**, 115014 (2007).
- [16] J. Wess and B. Zumino, Phys. Lett. B **37**, 95 (1971); E. Witten, Nucl. Phys. B **223**, 422 (1983).
- [17] S. L. Adler, Phys. Rev. **177**, 2426 (1969); J. S. Bell and R. Jackiw, Nuovo Cim. A **60**, 47 (1969).
- [18] C. Csaki, J. Heinonen, M. Perelstein and C. Spethmann, Phys. Rev. D **79**, 035014 (2009).
- [19] V. Barger, W. Y. Keung and Y. Gao, Phys. Lett. B **655**, 228 (2007).
- [20] A. Freitas, P. Schwaller and D. Wyler, JHEP **0809**, 013 (2008).
- [21] W. Y. Keung, I. Low and J. Shu, Phys. Rev. Lett. **101**, 091802 (2008).
- [22] A. Freitas and D. Wyler, JHEP **0611**, 061 (2006).
- [23] A. Belyaev, C. R. Chen, K. Tobe and C. P. Yuan, Phys. Rev. D **74**, 115020 (2006). *A CalcHEP model file for the Littlest Higgs model with T-parity*, <http://hep.pa.msu.edu/LHT/>
- [24] C. O. Dib, R. Rosenfeld and A. Zerwekh, JHEP **0605**, 074 (2006); L. Wang, W. Wang, J. M. Yang and H. Zhang, Phys. Rev. D **75**, 074006 (2007); M. Carena, J. Hubisz, M. Perelstein and P. Verdier, Phys. Rev. D **75**, 091701 (2007); Q. H. Cao, C. S. Li and C. P. Yuan, Phys. Lett. B **668**, 24 (2008); S. Matsumoto, M. M. Nojiri and D. Nomura, Phys. Rev. D **75**, 055006 (2007); D. Choudhury and D. K. Ghosh, JHEP **0708**, 084 (2007); Q. H. Cao and C. R. Chen, Phys. Rev. D **76**, 075007 (2007); S. Matsumoto, T. Moroi and K. Tobe, Phys. Rev. D **78**, 055018 (2008).
- [25] G. Cacciapaglia *et al.*, arXiv:0911.4630 [hep-ph]; G. Cacciapaglia, S. R. Choudhury, A. Deandrea and N. Gaur, arXiv:0911.4632 [hep-ph].
- [26] P. Meade and M. Reece, Phys. Rev. D **74**, 015010 (2006); L. T. Wang and I. Yavin, JHEP **0704**, 032 (2007); C. S. Chen, K. Cheung and T. C. Yuan, Phys. Lett. B **644**, 158 (2007); M. M. Nojiri and M. Takeuchi, Phys. Rev. D **76**, 015009 (2007); C. Kilic, L. T. Wang and I. Yavin, JHEP **0705**, 052 (2007); L. Wang, W. Wang, J. M. Yang and H. Zhang, Phys. Rev. D **76**, 017702 (2007); A. Datta *et al.*, Phys. Lett. B **659**, 308 (2008); J. Hubisz, J. Lykken, M. Pierini and M. Spiropulu, Phys. Rev. D **78**, 075008 (2008). A. Belyaev *et al.*, Pramana **72**, 229 (2009) [arXiv:0806.2838 [hep-ph]]; B. Bhattacharjee, A. Kundu, S. K. Rai and S. Raychaudhuri, arXiv:0910.4082 [hep-ph].
- [27] A. Pukhov, arXiv:hep-ph/0412191.
- [28] A. Freitas, P. Schwaller and D. Wyler, *A CalcHEP model file for the Littlest Higgs model with broken T-parity*, <http://www.itp.uzh.ch/~pedro/lht/>

- [29] S. Weinberg, *Physica (Amsterdam)* **96A**, 327 (1979); J. Gasser and H. Leutwyler, *Ann. Phys. (N.Y.)* **158**, 142 (1984); J. Gasser and H. Leutwyler, *Nucl. Phys.* **B250**, 465 (1985).
- [30] J. S. Schwinger, *Phys. Rev.* **82**, 664 (1951); J. S. Dowker and R. Critchley, *Phys. Rev. D* **13**, 3224 (1976); S. W. Hawking, *Commun. Math. Phys.* **55**, 133 (1977).
- [31] A. Manohar and H. Georgi, *Nucl. Phys. B* **234**, 189 (1984).
- [32] Vista/Sleuth Global Search for New Physics in 2.0fb^{-1} of $p\bar{p}$ Collisions at $\sqrt{s} = 1.96\text{ TeV}$,
http://www-cdf.fnal.gov/physics/exotic/r2a/20080228.vista_sleuth/publicPage.html
- [33] T. Goto, Y. Okada and Y. Yamamoto, *Phys. Lett. B* **670**, 378 (2009); F. del Aguila, J. I. Illana and M. D. Jenkins, *JHEP* **0901**, 080 (2009); M. Blanke *et al.*, arXiv:0906.5454 [hep-ph].
- [34] H. L. Lai *et al.*, *Phys. Rev. D* **51**, 4763 (1995); J. Pumplin *et al.*, *JHEP* **0207**, 012 (2002); D. Stump *et al.*, *JHEP* **0310**, 046 (2003).
- [35] P. Langacker, *Rev. Mod. Phys.* **81**, 1199 (2009); E. Salvioni, A. Strumia, G. Villadoro and F. Zwirner, arXiv:0911.1450 [hep-ph]; P. Langacker, arXiv:0911.4294 [hep-ph].
- [36] L. Randall and R. Sundrum, *Phys. Rev. Lett.* **83**, 3370 (1999); *Phys. Rev. Lett.* **83**, 4690 (1999).
- [37] P. Achard *et al.* [L3 Collaboration], *Phys. Lett. B* **572**, 133 (2003).
- [38] T. Aaltonen *et al.* [CDF Collaboration], *Phys. Rev. D* **78**, 012008 (2008).
- [39] H. S. Lee, *Phys. Lett. B* **674**, 87 (2009).
- [40] T. Sjöstrand, S. Mrenna and P. Skands, *JHEP* **0605**, 026 (2006).
- [41] J. Alwall *et al.*, arXiv:0712.3311 [hep-ph]; P. Skands *et al.*, *JHEP* **0407**, 036 (2004).
- [42] M. L. Mangano *et al.*, *JHEP* **0307**, 001 (2003).
- [43] M. R. Whalley, D. Bourilkov and R. C. Group, arXiv:hep-ph/0508110.
<http://projects.hepforge.org/lhapdf/>
- [44] M. Cacciari *et al.*, *JHEP* **0809**, 127 (2008).
- [45] S. Dittmaier, P. Uwer and S. Weinzierl, *Phys. Rev. Lett.* **98**, 262002 (2007); *Eur. Phys. J. C* **59**, 625 (2009).
- [46] G. Bevilacqua, M. Czakon, C. G. Papadopoulos and M. Worek, arXiv:1002.4009 [hep-ph].
- [47] J. Huston, arXiv:1001.2581 [hep-ph].

- [48] G. Aad *et al.* [The ATLAS Collaboration], arXiv:0901.0512 [hep-ex]; G. L. Bayatian *et al.* [CMS Collaboration], J. Phys. G **34**, 995 (2007).
- [49] Private communication with Bruce Mellado.
- [50] J. M. Campbell *et al.*, Phys. Rev. D **80**, 054023 (2009).